10-27-2022

Discovery and characterization of potent, efficacious, orally available antimalarial Plasmepsin X inhibitors and preclinical safety assessment of UCB7362

Martin A Lowe

Daniel E Goldberg

et al.

Journal of Medicinal Chemistry

pubs.acs.org/jmc

Article

Discovery and Characterization of Potent, Efficacious, Orally Available Antimalarial Plasmepsin X Inhibitors and Preclinical Safety Assessment of UCB7362

Martin A. Lowe, Alvaro Cardenas, Jean-Pierre Valentin, Zhaoning Zhu, Jan Abendroth, Jose L. Castro, Reiner Class, Annie Delaunois, Renaud Fleurance, Helga Gerets, Vitalina Gryshkova, Lloyd King, Donald D. Lorimer, Malcolm MacCoss, Julian H. Rowley, Marie-Luce Rosseels, Leandro Royer, Richard D. Taylor, Melanie Wong, Oliver Zaccheo, Vishal P. Chavan, Gokul A. Ghule, Bapusaheb K. Tapkir, Jeremy N. Burrows, Maëlle Duffey, Matthias Rottmann, Sergio Wittlin, Iñigo Angulo-Barturen, María Belén Jiménez-Díaz, Josefine Striepen, Kate J. Fairhurst, Tomas Yeo, David A. Fidock, Alan F. Cowman, Paola Favuzza, Benigno Crespo-Fernandez, Francisco Javier Gamo, Daniel E. Goldberg, Dominique Soldati-Favre, Benoît Laleu,* and Teresa de Haro*

Cite This: *J. Med. Chem.* 2022, 65, 14121−14143

Read Online

ACCESS | Metrics & More | Article Recommendations | Supporting Information

ABSTRACT: Plasmepsin X (PMX) is an essential aspartyl protease controlling malaria parasite egress and invasion of erythrocytes, development of functional liver merozoites (prophylactic activity), and blocking transmission to mosquitoes, making it a potential multistage drug target. We report the optimization of an aspartyl protease binding scaffold and the discovery of potent, orally active PMX inhibitors with in vivo antimalarial efficacy. Incorporation of safety evaluation early in the characterization of PMX inhibitors precluded compounds with a long human half-life ($t_{1/2}$) to be developed. Optimization focused on improving the off-target safety profile led to the identification of **UCB7362** that had an improved in vitro and in vivo safety profile but a shorter predicted human $t_{1/2}$. **UCB7362** is estimated to achieve 9 log 10 unit reduction in asexual blood-stage parasites with once-daily dosing of 50 mg for 7 days. This work demonstrates the potential to deliver PMX inhibitors with in vivo efficacy to treat malaria.

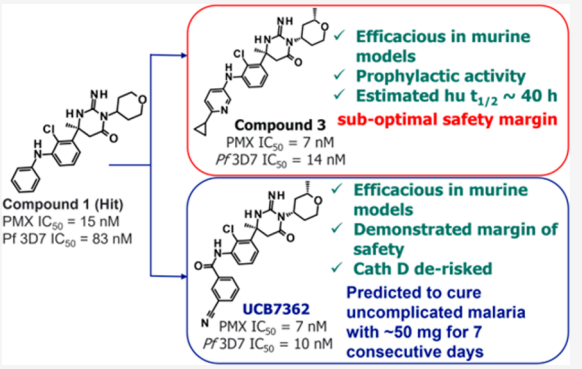

1. INTRODUCTION

Malaria is a serious mosquito-borne disease with an estimated 241 million cases and 627,000 deaths worldwide in 2020. This represents about 6% more cases and 12% more deaths compared to 2019, predominantly in children under the age of 5 in Africa.[1] This scourge is caused by protozoan parasites of the genus *Plasmodium*, among which *Plasmodium falciparum* (*Pf*) is the deadliest and most prevalent species in sub-Saharan Africa. There is a constant need for novel antimalarial medicines to complement existing artemisinin-dependent therapies, which are under pressure from resistance-conferring mutations. Moreover, the exploration of a new generation of cures that could drive the eradication of this disease is in high demand. With these goals in mind, focused target candidate and product profiles have been recently established to define the properties of effective antimalarials.[2]

Several studies have identified the essential role of apicomplexan aspartyl proteases in the virulence and transmission of malaria parasites, and their potential as new drug targets for next generation of antimalarial therapies.[3,4] New insights into structure-function properties of this key class of parasitic enzymes may aid in developing and optimizing specific inhibitors.[5] *P. falciparum* (*Pf*) encodes 10 aspartic proteases, known as plasmepsins (*Pf*PMI, II, and IV−X and Histo-aspartic protease (HAP)). PMV, PMIX, and Plasmepsin X (PMX) are the only plasmepsins essential during the red blood cell stages. PMI-IV are found in the digestive vacuole and are dispensable to parasite survival.[6] PMV serves as a maturase for proteins involved in host cell remodeling to be

Received: August 13, 2022
Published: October 10, 2022

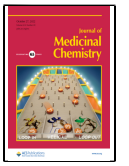

exported into the red blood cell's cytoplasm.[7] PMIX and PMX belong to a phylogenetic class involved in the maturation of rhoptry and micronemal proteins.[8] Merozoites egress from infected red blood cells in a two-step process that involves the degradation of the parasitophorous vacuole and the red blood cell membrane. Invasion of a new red blood cell takes 10−30 s and involves recognition of the red blood cell membrane, attachment, reorientation, and entry. The protein factors implicated in invasion and egress are packaged into two main secretory organelles in the merozoite, the rhoptries (invasion) and the exoneme (egress).[9,10]

PMIX and PMX were recently identified as new parasite targets for therapeutic intervention, as they carry out essential roles as maturases for rhoptry and microneme proteins, respectively.[11,12] PMX acts on secretory organelle proteins such as subtilisin-like serine protease 1 (SUB1), apical membrane antigen1 (AMA1), reticulocyte-binding protein homologs, and erythrocyte binding-like proteins that are responsible for both invasion and egress.[13]

PMX is expressed in the blood-stage schizont and merozoite stage; additionally, it is found in the gametocyte and liver stage of infection. Upon activation, the zymogens of PMX-like proteases form mature enzymes which promote invasion and egress of merozoites, transmission to mosquitoes, and merosome formation. This makes PMX an exciting multistage target of the *Plasmodium* life cycle. Phylogenetically, *Pf*PMIX and *Pf*PMX cluster with a group of aspartyl proteases conserved across the phylum of Apicomplexa including *Toxoplasma gondii* ASP3 which shares the same critical role in invasion and egress without impacting on intracellular growth.[8] Structural and biochemical studies are needed to investigate the active site's architecture, specificity, and affinity for the substrates and the inhibitors. Until recently, only homology models of the three-dimensional structure of *Pf*PMIX and *Pf*PMX have been constructed to aid in structure-based drug design.[14−17]

Cyclic guanidines are privileged aspartyl protease binding scaffolds.[18] The protonated, basic guanidine core binds to the catalytic aspartic acid diad found in the substrate binding site of the enzyme. In recent years, there have been several reports of molecules bearing this motif that have activity either as phenotypic inhibitors of malarial parasite growth, or direct inhibitors of plasmepsin activity (Figure 1). A screen of over 13,000 compounds by scientists at GlaxoSmithKline (GSK) looking for compounds with activity in a *Pf* 3D7 antimalarial assay revealed several hit compounds such as TCMDC-136879,[19,20] and demonstrated the potential of this motif to be used in antimalarial drug discovery. Subsequently, researchers have optimized this scaffold, with analogues such as CHWM-117.[21] Recently, the highly potent dual PMX/PMIX inhibitor WM382,[13] which has both demonstrated antimalarial activity in vitro and in vivo, has been described.

Cyclic acyl guanidine-based aspartyl protease inhibitors have been demonstrated to be robust druggable scaffolds that have been utilized in the development of human aspartyl proteases inhibitors such as BACE-1 and Renin.[22,23] The cyclic sulfonyl guanidine Verubecestat, was taken into phase 2 clinical trials for Alzheimer's disease.[24,25] As a result, the design of plasmepsin inhibitors that do not interact significantly with human counterparts presents a drug design challenge, as the plasmepsins share sequence homology with the human aspartic proteases, namely, Cathepsin D (Cat D), cathepsin E (Cat E), renin, and pepsin A. Specifically, Cat D and Cat E are relevant

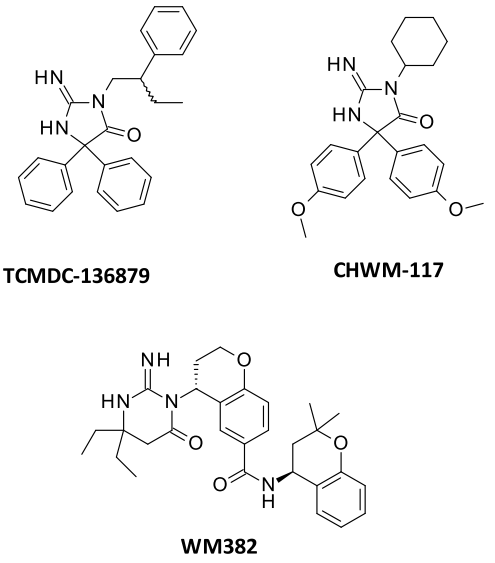

Figure 1. Cyclic acyl guanidines with antimalarial activity.

proteases because of their cellular location.[26] Cat D is a lysosomal enzyme found in many cells and Cat E is found in the gut and erythrocytes. Thus, inhibitory activity against Cat D and Cat E may be of toxicological concern.[27] With an overall PMX sequence identity of 19% to both Cat D and Cat E, the challenges for design to avoid these targets are augmented through a higher local sequence identity around the catalytic site and the promiscuity of the cyclic guanidine head group for the aspartic acid binding regions. Moreover, the loop movement observed in the binding sites directly below the aspartyl head groups is well established in the literature and typically changes conformation significantly in the presence of a small molecule compared to apo forms.[28] This offers both opportunities for dynamic differences between aspartyl proteases and challenges in accurate predictions.

A focussed library was designed to exploit the cyclic guanidine core based on the analysis of known literature compounds with activity against BACE and plasmepsins. We hypothesized this could deliver potent PMX inhibitors with good oral pharmacokinetics (PK) and a promising safety profile that could support the selection of a new antimalarial clinical candidate with a novel mode of action.

2. RESULTS AND DISCUSSION

2.1. Lead Optimization and In Vitro Characterization of Cyclic Acyl Guanidines with Activity against PMX. The focused library was tested for PMX inhibition in a fluorescence resonance energy transfer (FRET)-labeled subtilisin-like serine protease 1 (*Pf* SUB1) peptide substrate cleavage assay described by Pino et al.[11] From this screen, compound **1** was identified as a hit molecule with an half-maximal inhibitory concentration (IC_{50}) of 31 nM (Table 1). This compound was highly soluble and the log *D* was in an appealing range for further optimization. Further structure−activity relationship (SAR) exploration was undertaken to increase potency and reduce the metabolism of the compound (Table 1). Replacement of the metabolically labile distal benzene with a cyclopropyl pyridine reduced metabolism (compound **2**). Subsequent addition of a *cis*-methyl group onto the tetrahydropyran (THP) ring with *S*,*S* stereochemistry increased potency for all analogues made (see Table S3 in the

https://doi.org/10.1021/acs.jmedchem.2c01336
J. Med. Chem. 2022, 65, 14121−14143

Table 1. Early In Vitro Characterization of Compounds 1−5 and UCB7362

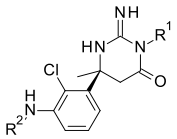

Compound	R^1	R^2	FRET *Pf*PMX/ *Pv*PMX IC_{50}[a] (nM)	FRET *Pf*PMIX IC_{50} (nM)	FRET *Pf*PMV IC_{50}[a] (nM)	*Pf*3D7[b] IC_{50} [free] (nM)	Hu Hep Clint (μL/min 10^6 cells)	FESSIF Solubility pH 5.8 (μM)	LogD	Off-target Screen[c] Hit Rate	Cat D / Renin /BACE IC_{50}[a] (nM)
1			15±6[d]/31±3[d]	-	2700±253[d]	83±1[e] [37]	28	1057	2.2	-	58±8[e] / -/ -
2		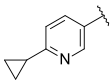	37±6[e]	-	-	-	3	1161	2.1	20%	1193±188[e]/ 1070[f]/ -[g]
3		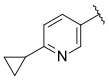	7±0[d,e,h]/ 7±1[d]	250[f]	> 10000[f]	14±1[e] [6]	6	959	2.5	20%	64±13[e]/ 180[f]/ 5000[f]
4		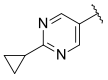	9±4[i] /10±1[e]	-	-	-	4	1372	2.0	14%	215±27[e]/ 2360[f]/ >10000[f]
5			32±10[d]	-	>5000[e]	-	4	-	1.2	5%	>10000[e]/ - / -
UCB7362		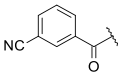	7±3[j,l]/8±0[d]	142[f]	-	10±5[k] [8]	4	1021	1.3	7%	3889±109[a]/ >10000[f]/ -[l]

[a]Data quoted ± standard deviation (SD). [b]Lactate dehydrogenase (LDH) assay IC_{50}, number in parentheses denotes the free concentration which binding to the proteins in the incubation media (albumax) is taken into account. [c]SafetyScreen 44 panel from Eurofins Discovery, Hit rate calculated as the % of targets with >50% binding or inhibition of enzymatic activity. [d]$N = 4$. [e]Values reported are means of two independent experiments. [f]Compounds were tested in duplicates (with $N = 1$). [g]52% inhibition at 10 μM. [h]90% inhibitory concentration (IC_{90}) = 72 ± 4 nM. [i]$N = 6$. [j]IC_{90} = 52 ± 5 nM. [k]$N = 7$. [l]64% inhibition at 10 μM.

Supporting Information) and led to the identification of lead compound **3**.

The absolute stereochemistry of the disubstituted THP ring was confirmed by vibrational circular dichroism (VCD) spectroscopy of the synthetic intermediate **17**. Compound **3** improved stability in human hepatocytes compared to compound **1** and maintained excellent solubility. An X-ray crystal structure of closely related pyrimidyl analogue **4**, confirmed that these compounds inhibit the enzyme orthosterically, through binding at the enzyme substrate binding site (Figure 2). The structure shows compound **4** in the predicted binding mode within the catalytic pocket and the cyclic guanidine binding directly to the catalytic diad. In addition to directly interacting with catalytic aspartic acids, compound **4** displaced the auto-inhibitory Arg244 that is seen in the apo structure (7RY7).[17] Although compounds **3** and **4** had improved metabolic stability, early safety profiling revealed a high hit rate of 20 and 14%, respectively, in an off-target selectivity panel of 44 antitargets (named "SafetyScreen 44" panel and hit rate defined by the % of targets with >50% binding or activity at 10 μM) including 24 GPCRs, 9 enzymes, 8 ion channels, and 3 transporters as defined by Bowes et al.[29] In addition, compound **3** inhibits the human aspartyl proteases Cat D and Renin with an IC_{50} of 64 and 180 nM, respectively.

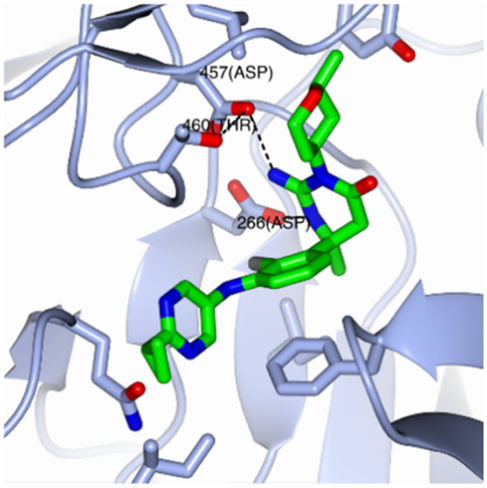

Figure 2. X-ray crystal structure of compound **4** bound to PMX (PDB ID: 8DSR). The dashed lines indicate the hydrogen-bonding interactions between the cyclic acyl guanidine with the catalytic aspartic acid diad. The figure was created using the PyMOL Molecular Graphics System, version 2.4, Schrödinger, LLC.

Greater selectivity was observed against BACE with an IC_{50} of 5000 nM (Table 1). Further optimization focused on

https://doi.org/10.1021/acs.jmedchem.2c01336
J. Med. Chem. 2022, 65, 14121−14143

Scheme 1. Synthesis of Plasmepsin Inhibitors 1−5 and UCB7362[a]

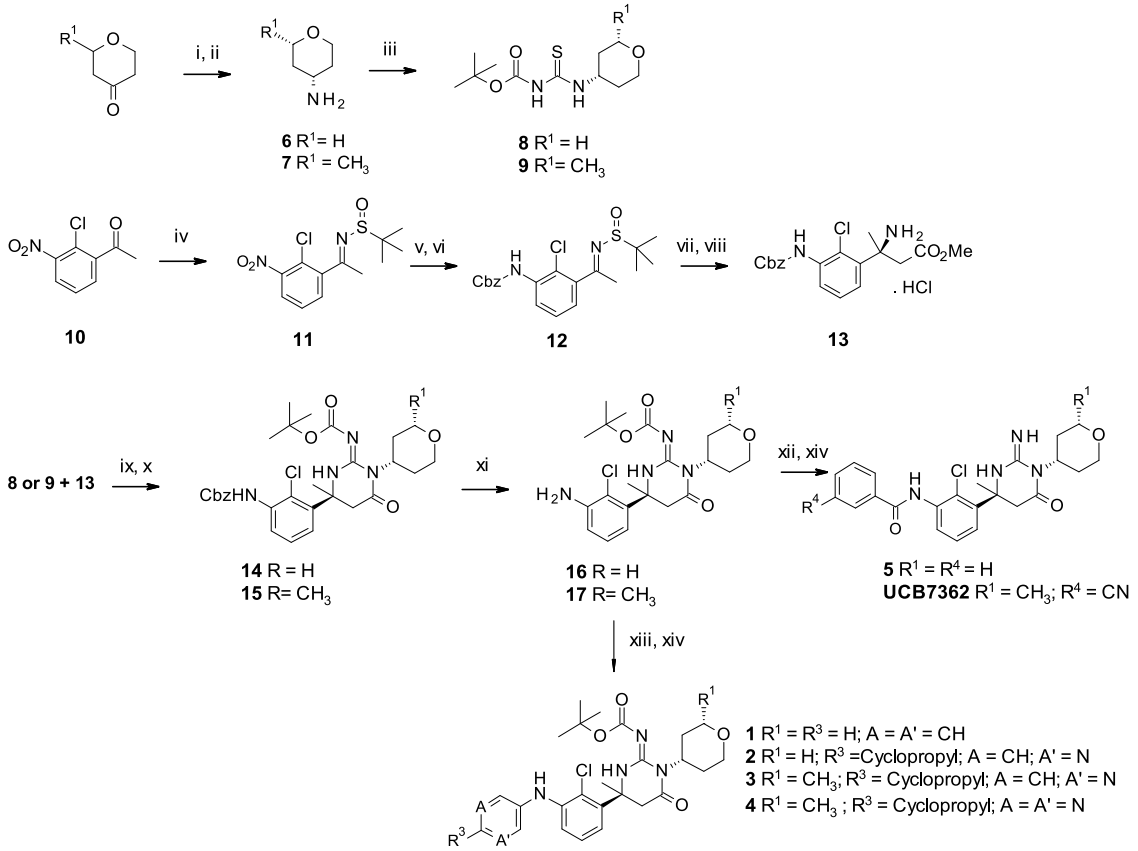

[a]Reagents and conditions: (i) $PhCH_2NH_2$, CH_3COOH, $NaBH_3CN$, MeOH, room temperature (RT); (ii) 20% Pd/C, MeOH, RT; (iii) NaH, trifluoroacetic anhydride (TFAA), S=C(NHCO$_2$*t*Bu), RT; (iv) (*R*)-2-methyl-2-propanesulfinamide, $Ti(OEt)_4$, THF, 75 °C; (v) Raney Ni, H_2, MeOH; (vi) *N*,*N*-diisopropylethylamine (DIPEA), $ClCO_2CH_2Ph$, THF, RT; (vii) CuCl, Zn, $BrCH_2CO_2Me$, THF 50 °C; (viii) 4 M HCl in dioxane, r.t; (ix) 1-ethyl-3-(3-dimethylaminopropyl)carbodiimide (EDCI), DIPEA, dimethyl formamide (DMF), RT; (x) KO*t*Bu, THF; (xi) H_2, MeOH, 20% Pd/C; (xii) acid chloride, pyridine, CH_2Cl_2, 0 °C; (xiii) phenyl boronic acid, $Cu(OAc)_2$, triethylamine (TEA), CH_2Cl_2, RT (for compound **1**) or aryl bromide, BrettPhos, BrettPhos Pd G3, NaO*t*Bu, 1,4-dioxane (for compound **2**−**4**); (xiv) TFA, CH_2Cl_2, RT (for compounds **1** and **5**) or 4 M HCl in dioxine, 1,4-dioxane, RT (for compounds **2**−**4** and **UCB7362**).

increasing off-target selectivity and reducing metabolic clearance (CL). Thus, replacement of the biaryl amine with an amide linker led to the identification of compound **5**, which substantially reduced the log *D* and the off-target hit rate. Final refinement through the addition of the potency-enhancing methyl group onto the THP ring and incorporation of a cyano group (CN) at the 3-position of the benzene ring (guided by insights from the X-ray crystal structure) led to the identification of **UCB7362**, which maintained the potency of compound **3** while improving metabolic stability and off-target selectivity. **UCB7362** also demonstrated an improvement in selectivity against Cat D and Renin with an IC_{50} of 3889 nM and >10,000 nM, respectively. Direct binding of **UCB7362** to the enzyme was demonstrated with SPR using immobilized PMX. The measured K_d of 5.5 nM was in close agreement with the potency measured in the enzyme and cell-based assays.

To understand the potential for these compounds to be active across multiple *Plasmodium* species, a *Plasmodium vivax* (Pv) FRET PMX substrate cleavage assay, analogous to that developed for *Pf* was used. It was found that our molecules were equipotent (Table 1), suggesting that these compounds should be equally active against the two most common malarial parasite species.

Finally, molecules identified in this chemical series are less potent when tested against other plasmepsin paralogs. For example, compound **3** was found to be less potent inhibitor of recombinantly expressed PMIX (250 nM) and PMV (>10,000 nM) (Table 1).

2.2. Synthetic Chemistry. A range of synthetic routes facilitating access to substituted cyclic guanidines has been described and reviewed.[30] Scheme 1 describes the route used to access compounds **1**−**5** and **UCB7362**. The critical step involves a coupling-cyclization protocol of *β* amino ester **13** and a thiourea (**8** or **9**), which could be prepared from the corresponding amino THP (**6** or **7** respectively). The cyclization proceeded in good yield, and the final compounds were prepared via coupling of the benzyloxy carbamate (Cbz)-deprotected aniline followed by boc-group removal and HCl or trifluoroacetic acid (TFA) salt formation.

2.3. Lead Compounds Profiling with Parasite Culture. The lead molecules were tested for activity in an asexual blood stage (ABS) assay of *Pf* parasites (3D7 strain) using a 384-well lactate dehydrogenase assay readout previously described by Gamo et al.[19] The most potent analogues inhibited parasite growth with potency in line with that measured in the recombinantly expressed FRET PMX substrate assay once the IC_{50} was adjusted for binding to the AlbuMAX assay media.

https://doi.org/10.1021/acs.jmedchem.2c01336
J. Med. Chem. 2022, 65, 14121−14143

Table 2. IC_{50} of Compound 1 and UCB7362 against Laboratory-Resistant Parasite Strains

		7G8	Dd2	K1	PH1263-C	TM90 C2B[b]	Dd2 048[c]	Dd2 DDD107498[d]	Dd2 DSM265[e]	Dd2 ELQ300[f]	Dd2 KAF156[g]
mutated locus	NF54[a]	*Pf*crt, *Pf*mdr1, *Pf*dhfr, *Pf*dhps	*Pf*crt, *Pf*mdr1, *Pf*dhfr, *Pf*dhps	*Pf*crt, *Pf*mdr1, *Pf*dhfr, *Pf*dhps	*Pf*CRT	*Pf*crt, *Pf*mdr1, *Pf*dhfr, *Pf*dhps, $Pfcytb_{Q0}$	*Pf*pi4k[i]	*Pf*eef2[i]	*Pf*dhodh[i]	*Pf*cytB[i]	*Pf*carl[i]
1 IC_{50}[h] (nM)	107	79	59	112		62	87	82	78	96	83
UCB7362 IC_{50}[h] (nM)	34.6	24	18	33	18	15	20	22	22	17	19

[a]Sensitive strain. [b]See ref 34. [c]See ref 35. [d]See ref 36. [e]See ref 37. [f]See ref 38. [g]See ref 39. [h]72 h [3H] hypoxanthine incorporation assay, mean values from two independent biological replicates the majority of the individual values varied not more than 10% (maximum 17% for Dd2). A replicate data for **UCB7362** can be found in the Supporting Information including data of reference compounds (chloroquine and artesunate), number of replicates, and SD. [i]Genetically engineered *P. falciparum* strains. Mutations were introduced in the Dd2 wild-type strain.

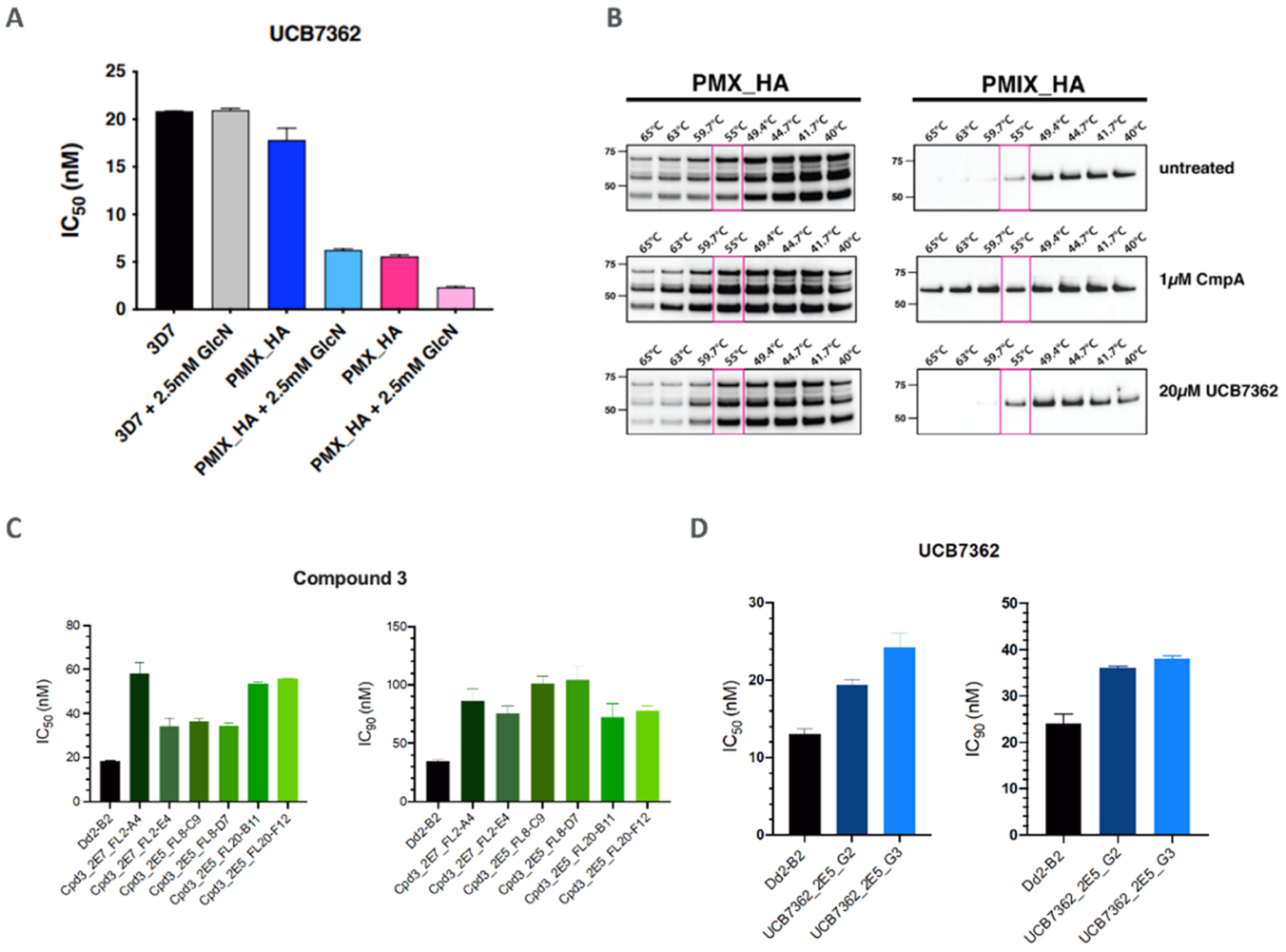

Figure 3. *Pf*PMX as a target and resistance mediator of **UCB7362**. (A) **UCB7362** IC_{50} of 3D7, 3D7-PMIX-HA knockdown, and 3D7-PMX-HA knockdown parasites in the presence and absence of 2.5 mM Glucosamine (GlcN). Half-maximal inhibitory concentration (IC_{50}) values are shown as mean ± standard error (SE). (B) Immunoblots probed with a-HA mAb in 3D7-PMX_HA and 3D7-PMIX_HA parasites. Untreated and CmpA (WM382)-treated samples served as negative and positive controls, respectively. Compound **3** (Cpd3) (C) and **UCB7362** (D) IC_{50} and IC_{90} values of resistant Dd2-B2 parasites derived from in vitro selections with compound **3** and **UCB7362**, respectively. IC_{50} and IC_{90} values are shown as mean ± standard error of the mean (SEM).

Both the initial hit molecule **1** and **UCB7362** were tested for efficacy against a panel of laboratory-resistant *Pf* strains (Table 2). The compounds were found to be inhibitors of parasite growth across all strains tested regardless of geography[31] and resistance profile and showed potency similar to that tested in the LDH 3D7 asexual blood stage assay.[32] The compounds demonstrated no cross-resistance when tested against drug-resistant *Plasmodium* strains containing mutations generated with other compounds in development.[33−39]

In-cell target engagement of **UCB7362** against PMIX and PMX was explored using *Pf* 3D7-PMX-HA and 3D7-PMIX-HA parasites cell lines which have an HA epitope and use the glucosamine (GlcN) inducible glmS ribozyme to allow knockdown expression of PMX and PMIX, respectively

https://doi.org/10.1021/acs.jmedchem.2c01336
J. Med. Chem. 2022, 65, 14121−14143

(Figure 3A).[13] The IC_{50} of **UCB7362** was significantly reduced when PMX expression was decreased.[40] Cellular thermal shift assays (CETSA) confirmed binding of **UCB7362** to PMX, but no binding was seen to PMIX (Figure 3B).[41,42] In addition, recombinant PMIX was expressed and purified, and used in a peptide substrate cleavage assay to measure the activity of **UCB7362**.[13,16] **UCB7362** was substantially more potent against PMX than PMIX with an IC_{50} of 7 nM for the former compared to 142 nM for the latter.

2.4. *P. falciparum* Resistance Selection Studies. The emergence of drug-resistant *P. falciparum* parasite strains is a major concern to address when developing new antimalarials.[43,44] To determine the minimum inoculum of Dd2-B2 parasites needed to obtain a single event of resistance (MIR),[45] we conducted selections with compound **3** using varying starting parasite inocula of 2×10^5 (per well × 24 wells in a 24-well plate) and 2×10^7 (per well × 3 wells in a 6-well plate). The IC_{50} of compound **3** was determined to be 22.5 ± 0.3 nM (based on two independent assays in duplicate), and these selections employed a consistent drug pressure of 3× IC_{50} over 60 days. Resistant parasites were detected by flow cytometry within 20 days, with most of the resistant cultures becoming positive around day 30. In total, nine out of 24 of the 2×10^5 wells and all three of the 2×10^7 wells became positive. Considering the lower inocula, this corresponded to a minimum inoculum of resistance (MIR) value of 5.3×10^5 ($2 \times 10^5 \times 24/9$), representing the number of parasites required to yield a single instance of resistance.

Drug dose−response assays with each of the three 2×10^7 wells and five of the 2×10^5 wells revealed similar levels of resistance, in the range of 1.7- to 2.6-fold and 2.0- to 2.4-fold IC_{50} and IC_{90} increases, respectively, compared to the parental Dd2-B2 parasites (Figure 3C). Cloned resistant parasites were then generated from three bulk cultures, and dose−response profiling of six clones showed a range of 2- to 3-fold IC_{50} increases. Three clones (Cpd**3**_2E7_ FL2-A4, Cpd**3**_2E5_ FL20-F12, and Cpd**3**_1E5_ FL8-C9) were then selected for whole-genome sequencing, the first two of which had slightly higher IC_{50} values. Sequencing analysis revealed that these first two clones contained a 3-fold amplification of overlapping segments of chromosome 8. Cpd**3**_2E7_ FL2-A4 amplified an 83 kb segment spanning Pf3D7_0806500 to Pf3D7_0808500, whereas Cpd**3**_2E5_ FL20-F12 amplified an internal 29 kb segment spanning PF3D7_0807700 to PF3D7_0808400. Common to both amplicons was the PMX gene (PF3D7_0808200), with three copies in each mutant clone. No single-nucleotide polymorphisms (SNPs) were observed in either clone when compared to the parental Dd2-B2 line. Of note, Cpd**3**_2E5_ FL8-C9 did not contain amplification of PMX. Instead, this clone harbored a nonsynonymous S503Y mutation in PF3D7_0507500 that encodes subtilisin-like serine protease 1 (SUB1), which like PMX, is involved in the enzymatic pathway regulating parasite egress from or invasion of host red blood cells.

Of note, PMX is known to control the maturation of SUB1 in exoneme secretory vesicles, with SUB1 itself being a key regulator of merozoite surface proteins and cysteine proteases.[6,46]

An additional selection was conducted with **UCB7362** using 2×10^5 Dd2-B2 parasites in each well of a 96-well plate. The IC_{50} was determined to be 10.1 ± 0.23 nM (based on two independent assays in duplicate), and this selection employed a consistent drug pressure of 3× IC_{90} (42.9 nM) over 60 days. Resistant parasites were detected by flow cytometry within 21 days. In total, 2 out of 96 of the 2×10^5 wells became positive. This corresponded to a MIR value of 9.6×10^6 ($2 \times 10^5 \times 96/2$). Drug dose−response profiling of these two wells, G2 and G3, showed a 1.5−1.9× IC_{50} shift and a 1.5−1.6× IC_{90} shift (based on four independent assays in duplicate) (Figure 3D). Whole-genome sequencing of the G2 genome revealed copy number variations (CNVs) gained by 2-fold in PF3D7_0808100 and PF3D7_0808300, which contain the putative AP-3 complex subunit delta and ubiquitin regulatory protein respectively. PF3D7_0808100 and PF3D7_0808300 are both 3-exon genes located on chromosome 8. Notably, the G2 genome additionally showed a CNV gained by ∼2-fold in a 14 kb region containing the Plasmepsin X gene on chromosome 8, consistent with the low IC_{50} fold shift observed in the bulk culture (Figure 3D). No SNPs were observed in the G2 genome. Of note, G3 did not contain amplification of PMX, but rather an SNP, a nonsense mutation (E873*) in PF3D7_0521300. PF3D7_0521300 encodes a putative zinc finger protein, a 3-exon gene on chromosome 5. This and the aforementioned selection suggest that PMX is an important genetic determinant of resistance in *Pf* to both compound **3** and **UCB7362**.

2.5. In Vitro Killing Rate of UCB7362. The parasite killing profile for **UCB7362** was determined using an in vitro limiting dilution technique to quantify the number of parasites that remain viable after drug treatment at a concentration of 10× IC_{50} (Figure 4).[47] The killing profile showed a lag phase

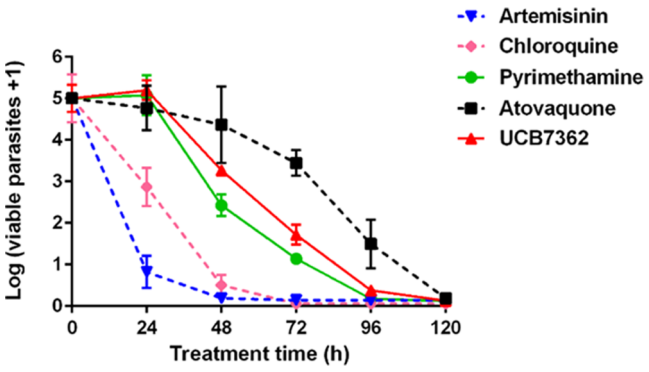

Figure 4. In vitro antimalarial killing rate of **UCB7362.** Parasites were treated with **UCB7362** or pyrimethamine at 10× IC_{50} and the number of viable parasites was quantified in one experiment with four technical replicates (±SD). Data from artemisinin, chloroquine, and atovaquone are retrieved from previously generated data and shown for comparative purposes (dash lines).

of 24 h, which may be consistent with the egress inhibition mode of action, and overall, the killing profile was similar to the known antimalarial pyrimethamine. All parasites in the initial inoculum were killed after two life cycles of drug treatment with a logPRR (parasite reduction ratio) of 3.2. Similar PRR values were obtained with other plasmepsin inhibitor analogues tested (data not shown), which is consistent with the mechanism of action.

2.6. In Vivo Efficacy of Compound 3 and UCB7362. The efficacy of **UCB7362** and compound **3** against erythrocyte asexual stages of *Pf* in vivo was evaluated in a standardized *P. falciparum* humanized mouse model.[48] Both compounds cleared parasitemia from peripheral blood in a dose-dependent manner when administered orally (Figure 5A,C). Flow

https://doi.org/10.1021/acs.jmedchem.2c01336
J. Med. Chem. 2022, 65, 14121−14143

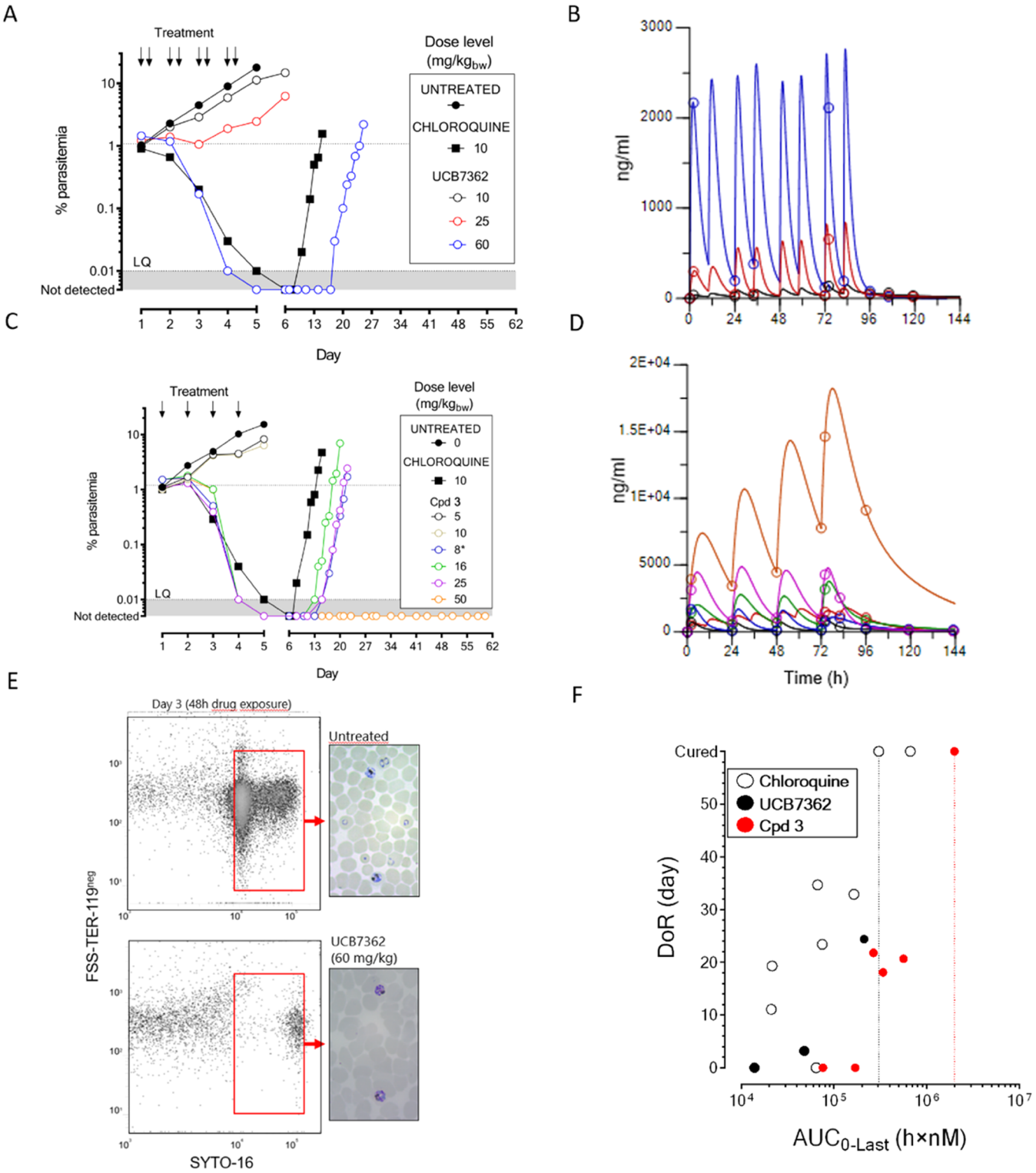

Figure 5. (A, C) *Pf*SCID mouse model efficacy of **UCB7362** (bis in die (bid) oral administration for 4 days with the second administration 10 h after the first one) and compound **3** (daily oral administration for 4 days). Parasitemias below the detection limit are represented as points at the bottom of the plot in the gray area. (B, D) Pharmacokinetic modeling of the concentration of **UCB7362** and compound **3** in whole blood. Open symbols represent the experimental values of concentration in blood. Solid lines represent the predicted concentrations using a two-compartment pharmacokinetic model with WinNonLin 8.2. (E) Population distribution of asexual blood stage *P. falciparum* assessed by flow cytometry and microscopy. Data from a representative control and treatment individual. (F) Analysis of parasite killing in vivo by measuring DoR. Vertical dashed lines represent the lowest concentration at which the cure of an individual was observed. Data points at DoR = 0 and DoR = cured represented individuals for which parasitemia was not inhibited below the parasitemia at treatment inception at any time during the study (i.e., treatment failure) or individuals with no detectable parasitemia at day 60 (i.e., cured individuals), respectively.

https://doi.org/10.1021/acs.jmedchem.2c01336
J. Med. Chem. 2022, 65, 14121−14143

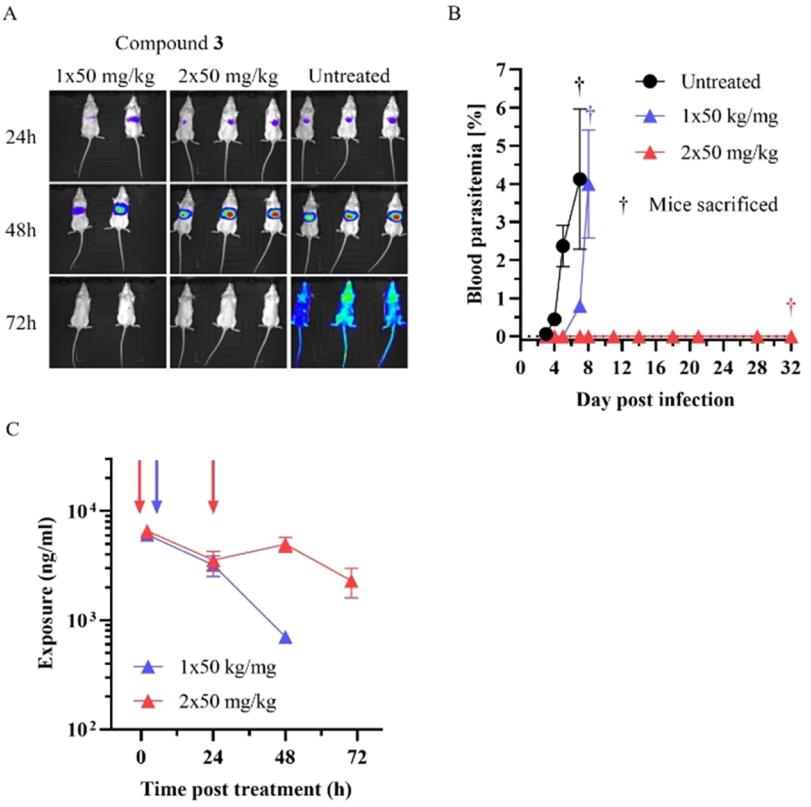

Figure 6. (A) In vivo efficacy of compound **3** in a prophylactic liver mouse model for rodent *P. berghei* malaria, orally exposed to one (at 24 h post-infection) or two (at 24 and 48 h post-infection) doses of 50 mg/kg. (B) Ventral view images of B6/Albino mice (24, 48, and 72 h after infection) with 20,000 luciferase expressing sporozoites. Heat maps of mice represent the intensity of bioluminescence. (C) Average blood parasitemia obtained from microscopy reading of blood smears collected from day 3 post-infection. Mean blood concentration after compound administration.

Table 3. Physicochemical and ADME Properties

compound	3	UCB7362
MW (g/mol, free base)	468	480
salt form	hydrochloride	hydrochloride
pK_a	8.4	8.1
log *D* pH 7.4/log *P*	2.5/3.4	1.3/2.1
solubility (μM) FaSSIF/FeSSIF	865/960	1156/1021
clint hepatocytes human/mouse/rat /dog/cynomolgus monkey (μL/min/10^6 cells)	6/23/34/5/21	4/42/66/7/24
plasma protein binding (%) human/mouse/rat/dog/cynomolgus monkey	96.1/97.7/95.5/ 93.6/98.7	74.1/62.7/55.7/ 41.2/70.8
AlbuMAX binding (%)	58.3	23.0
hepatocytes binding (%)	62.6	14.1
blood−plasma ratio human/mouse/rat/dog/cynomolgus monkey	0.75/0.93/1.19/ 0.92/0.69	0.97/1.20/1.16/1.18
Caco-2 passive permeability pH 6.5 > 7.4 (nm/s)	ND (low recovery)	25
Caco-2 efflux ratio pH 7.4 > 7.4 2/10/50 μM	34/7/3	411/169/85

cytometry and microscopy analysis showed a relative accumulation of circulating mature schizonts compared to untreated controls on day 3 of the assay (Figure 5E) after two cycles of drug exposure. This suggests that the final maturation/egress of merozoites and reinfection of naïve human erythrocytes were the most sensitive stages of the parasite to **UCB7362** and compound **3**. Pharmacokinetic modeling of the concentrations of **UCB7362** and compound **3** in blood showed rapid absorption with no accumulation except in the mouse treated with compound **3** at 50 mg/kg (Figure 5B,D). The data showed that **UCB7362** and compound **3** induced a parasite clearance comparable to chloroquine in the same experimental system. Analysis of parasite killing in vivo (recrudescence period (DoR))[49] showed that compound **3** was as efficacious as chloroquine and curative at 50 mg/kg (area under the curve $(AUC)_{o\rightarrow Last} = 2 \times 10^6$ nM h) although less potent than this reference marketed compound (Figure 5F). Despite the small sample size, the PK/PD data on DoR pointed to the total time above a threshold concentration in blood as an important PK driver of efficacy. Thus, the mice treated with either **UCB7362** or compound **3** for which exposure in blood lasted for only about 96 h showed recrudescence at a very similar DoR. This would be consistent with a requirement for the continuous presence of the drug in blood for a minimum time to be curative by blocking egress and reinfection.

2.7. Prophylactic Liver Mouse Model. The efficacy of compound **3** in a prophylactic liver mouse model for rodent

https://doi.org/10.1021/acs.jmedchem.2c01336
J. Med. Chem. 2022, 65, 14121−14143

Table 4. Summary of Mean Pharmacokinetic Parameters for Compound 3 and UCB7362 Obtained after Intravenous (IV) and Oral Administration to Preclinical Species and Predicted In Vivo Clearance from Incubated Hepatocytes

compound	3		UCB7362		
species	Sprague Dawley rat	Beagle dog	Sprague Dawley rat	Beagle dog	Cynomolgus monkey
IV dose level (1 mg/kg)					
CL (mL/(min kg))	20.5	7.28	43.9	12.9	18.9
V_{ss} (L/kg)	11.7	12.5	5.72	8.20	3.07
AUC (nM h)	1750	3220	793	2900	1906
$t_{1/2}$ (h)	7.0	20.0	2.1	17.0	4.1
PO dose level (10 mg/kg)					
C_{max} (nM)	736	2730	246	4340	2563
T_{max} (h)	8	8	3	0.5	1
AUC (nM h)	16400	62200	1410	34500	7375
apparent bioavailability (%)	94	193	11	120	39
in vitro predicted CL					
hepatocytes (mL/(min kg))	28.6	7.72	53.8	16.3	18.3

Plasmodium berghei (Pb) malaria was also assessed, using a genetically modified strain that utilizes bioluminescence to detect parasites (Figure 6). The antimalarial efficacy against the liver stages of the parasite was evaluated in mice infected with 20,000 sporozoites following administration of either one or two oral doses of 50 mg/kg administered at 24 h, and 24 and 48 h post-infection respectively. The impact on liver infection was assessed by live monitoring of luminescence and the emergence of parasites in the blood visualized via microscopic analysis of Giemsa-stained blood smears (on days 3−30 post-infection). Neither treatment regimen with compound **3** decreased liver infection on days 1 and 2 (Figure 6A). A single dose of compound **3** delayed the emergence of blood stage parasites, detected on day 8 post-infection, vs day 3 in the untreated control mice (Figure 6B). However, the double treatment on two consecutive days post-infection prevented the emergence of blood stage parasites (Figure 6B). These mice were deemed cured as parasites could not be detected after 30 days. The exposure profile suggests that a total concentration above 1 μg/mL at 24 h post-infection is necessary to clear the infection (Figure 6C). This is consistent with the findings reported previously about the prophylactic action of WM382 due to exoerythrocytic merosomes found to be not viable and noninfectious.[13]

2.8. Absorption−Distribution−Metabolism−Excretion (ADME) Properties and Pharmacokinetics of Compound 3 and UCB7362. The druglike properties and pharmacokinetics of **UCB7362** and compound **3** were further explored. Both compounds are basic and highly soluble in the hydrochloride salt forms (around 1 mM in FaSSIF and FeSSIF) (Table 3). In plasma, protein binding in humans was 74.1 and 96.1% for **UCB7362** and compound **3**, respectively. In human hepatocytes, the unbound intrinsic clearance was moderate for compound **3** (16 μL/min/10^6 cells) and lower for **UCB7362** (5 μL/min/10^6 cells). In nonclinical species, the clearance in incubated hepatocytes is moderate in dog and moderate-high in mouse, rat, and cynomolgus monkey. Screening of cytochrome P450 (CYP450) inhibition with **UCB7362** and compound **3** suggests a low risk of drug−drug interaction (DDI) as perpetrators since for the five isoforms tested at 20 μM, inhibition was ≤20% with the only exception of CYP2D6 for **UCB7362**, that at 20 μM, 45% of inhibition was observed. Both compounds show a high efflux ratio in Caco-2 cells, suggesting the involvement of transporters. In Caco-2 cells, the apical basolateral permeability increases and the efflux ratio decreases, when the concentration of compound in the incubation is increased. Due to the high solubility of these compounds, saturation of efflux transporters in the human gut is expected. The apparent passive permeability of **UCB7362** at 10 μM in Caco-2 cells (pH 6.5 > pH 7.4) in the presence of transporter inhibitors elacridar (10 μM) and MK-751 (100 μM) was 25 nm/s, suggesting moderate permeability (estimated human effective permeability of 0.98×10^{-4} cm/s).

In vivo pharmacokinetics studies were performed in rat and dog with compound **3** and **UCB7362** (Table 4). For **UCB7362**, the pharmacokinetic profile in cynomolgus monkey was also explored. Compound **3** showed low clearance in rat and dog (<30% of liver blood flow (LBF)), while **UCB7362** showed moderate clearance in dog and cynomolgus monkey (<50% LBF) and moderate-high in rat (∼60% LBF). For both compounds, and all species, the in vivo clearance was well predicted from in vitro intrinsic clearance determined in hepatocytes. The volume of distribution of **UCB7362** was high, ranging from 3 L/kg in cynomolgus monkey to 8 L/kg in dog. Compared with **UCB7362**, the volume of distribution in rat and dog was higher for compound **3** (around 12 L/kg) consistent with its higher lipophilicity and basicity. In those species, the terminal half-life of compound **3** was also longer than **UCB7362**.

The oral pharmacokinetic studies were performed with 10 mg/kg of drug using 0.1% of methylcellulose and 0.1% of Tween 80 as vehicle. In dog, apparent bioavailability was higher than 100% suggesting nonlinear clearance. For rat, apparent bioavailability was close to 100% for compound **3** but only 11% for **UCB7362**. Bioavailability for **UCB7362** was 39% in cynomolgus monkey. For compound **3**, the estimated fraction absorbed in rat and dog was ∼100%. For **UCB7362**, the estimated fraction absorbed was 50% for rat, 70% for cynomolgus monkey, and 100% for dog.

2.9. In Vitro Metabolism of Compound 3 and UCB7362. In vitro metabolite profiling of **UCB7362** and compound **3** was performed in rat, dog, cynomolgus monkey, and human hepatocytes. For both **UCB7362** and compound **3**, there was coverage of all of the human metabolites in the preclinical species. The main sites of metabolism for both molecules are either on the distal ring (cyanobenzamide for **UCB7362** or cyclopropylpyridyl for compound **3**) or the methyl THP and comprise the oxidative metabolic pathways. Based on relative peak areas, the major metabolite of

https://doi.org/10.1021/acs.jmedchem.2c01336
J. Med. Chem. 2022, 65, 14121−14143

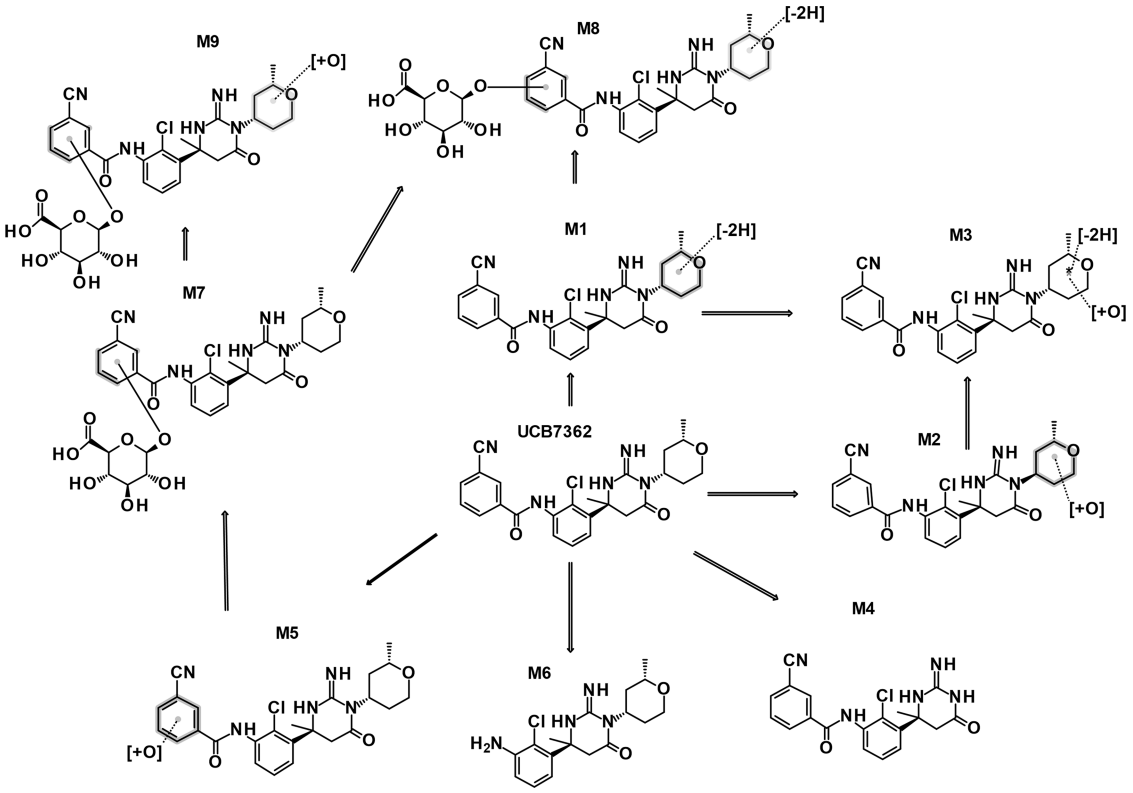

Figure 7. In vitro metabolism summary of **UCB7362** following incubation in human, cynomolgus monkey, dog, and rat hepatocytes.

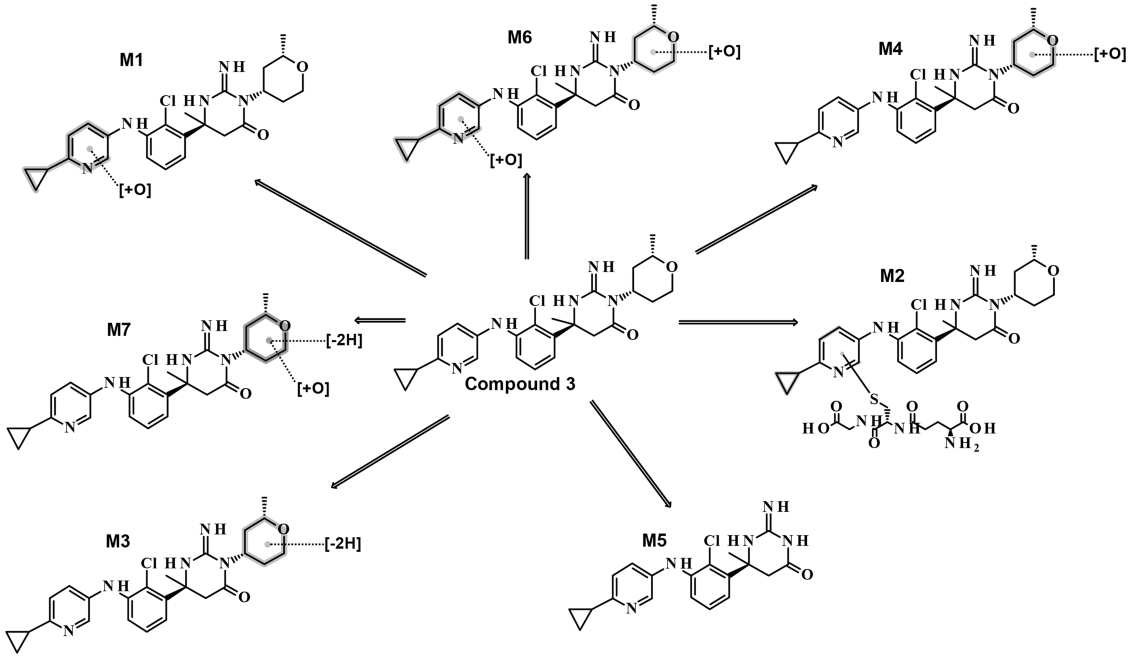

Figure 8. In vitro metabolism summary of compound **3** following incubation in human, cynomolgus monkey, dog, and rat hepatocytes.

UCB7362 in human hepatocytes was desaturated THP (M1), which was also significant in the preclinical species. Minor human metabolites are composed of the hydroxylated THP (M2) and desaturated THP (M3), plus the dealkylated THP moiety (M4). Hydroxylation of the distal ring (M5) and hydrolysis of the amide to the aniline (M6) were only detected in dog and human. Metabolite profiles in the preclinical species also include phase II glucuronidation of M5 (M7). In rat, metabolites M8 and M9 are detected, representing combinations of M7 and either M1 or M2, respectively (Figure 7).[50] Based on relative peak areas, the major metabolite of compound **3** in human hepatocytes was the hydroxylated cyclopropyl pyridine (M1), which was also significant in the preclinical species. Phase II metabolism of the distal ring results in the formation of a glutathione (GSH) (M2) metabolite in all species. Numerous oxidative metabolites of

https://doi.org/10.1021/acs.jmedchem.2c01336
J. Med. Chem. 2022, 65, 14121−14143

THP were also observed across all species (M3, M4, and M7), with further metabolism resulting in the dealkylation of the THP (M5). A combination of oxidative metabolites of the distal ring and the THP was also detected (M6) (Figure 8).

2.10. Human Pharmacokinetic Prediction of UCB7632 and Compound 3. An initial estimate of the human pharmacokinetics, assuming monocompartmental behavior, was performed with **UCB7362** and compound **3**. Using unbound Clint measured in hepatocytes and applying nonrestrictive well-stirred equations,[51] a good correlation between predicted and observed in vivo CL in preclinical species was noted for all tested preclinical species with **UCB7362** (Table 4). Therefore, this method was used to predict the human clearance of **UCB7362**. For compound **3**, which is slightly more basic and is highly bound to plasma proteins, Berezhkovskiy's[52] modification of the well-stirred model considering the pH gradient of hepatocyte vs plasma and drug ionization was better correlated with the clearance observed in nonclinical species (Table 4). Accordingly, Berezhkovskiy's method was used to predict human clearance of compound **3**. Hepatic metabolic clearance was considered the main elimination pathway for both compounds. Volume of distribution was estimated from preclinical species by the unbound V_{ss} equivalence approach.[53] For **UCB7362**, the fraction absorbed in the portal vein and constant of absorption (K_a) were estimated from permeability data generated in Caco-2 cells, using the equations described by Sugano and Terada.[54] The estimation of fraction absorbed (80%) was consistent with the calculated values from the in vivo PK in nonclinical species (100% in dog, 70% in monkey). For compound **3**, due to low recovery in the Caco-2 cell assay (<50%), the Sugano and Terada approach used for **UCB7362** to estimate the constant of absorption could not be applied, and accordingly, for compound **3**, a K_a value of 1 h^{-1} was assumed for the human prediction. The absorption in the portal vein in humans for compound **3** was estimated to be 100%, which is the estimated value from in vivo pharmacokinetic studies in rat and dog. Bioavailability for both compounds was calculated as the product of the fraction absorbed, and the fraction metabolized in the liver was calculated from hepatic clearance. Overall, the prediction suggests a longer half-life (40 h) and slightly higher bioavailability (85%) for compound **3** than for **UCB7362** (14 h and 70%) (Table 5).

Table 5. Summary of Predicted Human Pharmacokinetic Parameters for UCB7362

PK parameter	units	predicted estimate **UCB7362**	predicted estimate compound **3**
CL	mL/(min kg)	2.7	2.6
V_{ss}	L/kg	3.2	9.3
$t_{1/2}$	h	~14	~40
K_a	h^{-1}	0.6	1
bioavailability	%	70	85

To predict the dose that would be required in human patients, it was assumed that it is essential to be above a threshold of PMX inhibition of 90%. Therefore, the plasma concentration threshold (90% effective concentration (EC_{90})), calculated from the IC_{90} of PMX inhibition assay, was 0.61 μM (0.024 μM free) and 0.10 μM (0.025 μM free) for compound **3** and **UCB7362**, respectively. Considering that the in vitro PRR showed a lag phase of 24 h and a log(PRR) of 3.2 over 48 h, it was estimated that, to reduce the parasite population by 9 log, the exposure of the compound should be above the 90% inhibition threshold for 7 days.

For compound **3**, with a half-life estimated of ~40 h, the prediction of dose for three consecutive daily doses was explored. However, for **UCB7362** with a shorter predicted half-life (~14 h), the predicted dose for once-daily treatment for 7 days was considered. Using the estimates in human pharmacokinetics and inhibition threshold value, it was predicted that for compound **3**, a daily dose for 3 days of 550 mg would reduce the parasite population above 9 logs. To reach a similar effect on parasitemia with **UCB7362**, a daily dose of 50 mg for 7 days would be required. The C_{max} and integrated AUC in humans for compound **3** and **UCB7362** following these treatments were calculated using the predicted PK parameters of a monocompartmental model. For compound **3**, a C_{max} of 4.6 μM (0.18 μM free) and integrated AUC of 405 μM h are predicted in human for a treatment paradigm of three consecutive daily doses of 550 mg. For **UCB7362**, a C_{max} of 0.48 μM (0.13 μM free) and integrated AUC of 56.5 μM h (14.6 μM h free) are predicted in human for a treatment paradigm of 7 consecutive daily doses of 50 mg.

2.11. Preclinical Safety Assessment of Compound 3 and UCB7362. Having demonstrated that compound **3** and **UCB7362** potentially have the potency and exposure required to achieve efficacy in the clinic, we sought to establish whether their safety profile would support further development as a potential preclinical candidate for the treatment of malaria. Compound **3** showed an IC_{50} of 16 μM against a HepG2 cell line and showed inhibitory activity across multiple cardiac ion channels in patch clamp assays (human ether-a-go-go related gene (hERG) IC_{50}: 14 μM, Nav1.5 IC_{50}: 5−13 μM with rate dependence, Nav1.8 IC_{50}: 8 μM, Cav1.2 IC_{50}: 27 μM, Kv1.5 IC_{50}: 5 μM, Kv4.3 IC_{50}: 28 μM). As a result, we sought to understand the cardiovascular safety profile in more detail by testing compound **3** in vivo in anesthetized guinea pigs dosed with three consecutive incremental intravenous infusions of 15 min each (Figure 9). We observed dose/exposure-dependent

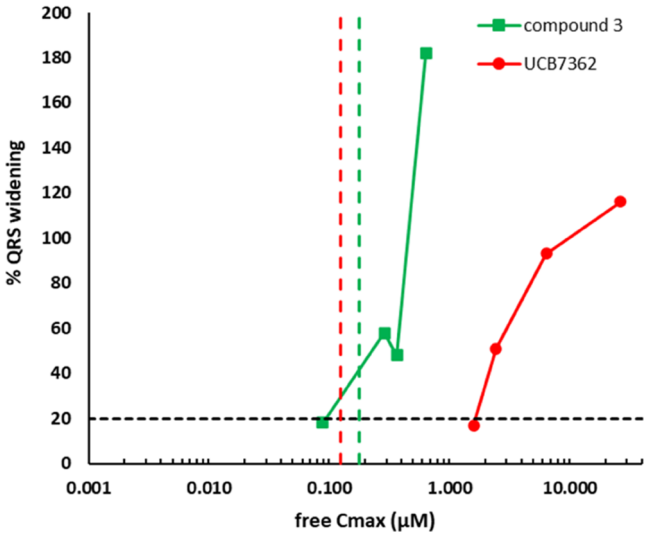

Figure 9. QRS widening induced by intravenous infusion of compound **3** and **UCB7362** (squares and circles, respectively) in anesthetized guinea pigs. The horizontal bar represents 20% QRS widening, threshold for safety concern. The vertical bars represent the predicted free C_{max} in man.

https://doi.org/10.1021/acs.jmedchem.2c01336
J. Med. Chem. 2022, 65, 14121−14143

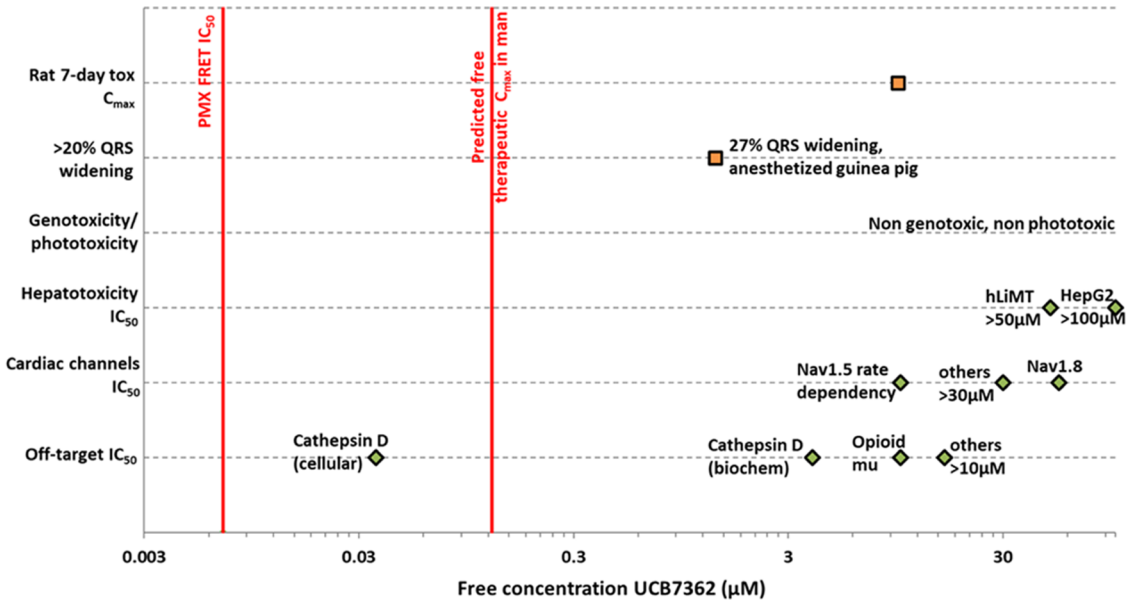

Figure 10. Composite preclinical safety profile data of **UCB7362** in relation to the estimated free therapeutic concentration for 7 daily dose treatment.

QRS widening with an 20% effective concentration (EC_{20}) of 90 nM (unbound plasma concentration producing 20% QRS widening). This effect was accompanied by dose-dependent decreases in heart rate, arterial blood pressure, and cardiac contractility.

As a result, further development of compound **3** was halted as an acceptable margin of safety could not be achieved.

The improved selectivity of **UCB7362** compared to compound **3**, assessed in the SafetyScreen 44 panel,[29] was further confirmed in a wider panel of in vitro secondary pharmacology assays containing 129 additional off targets. **UCB7362** showed a lower hit rate of (2%) compared to compound **3** (7%). **UCB7362** was not cytotoxic at concentrations up to 100 μM and only showed Nav1.5 rate dependent-inhibitory activity in a panel of nine cardiac ion channel patch clamp assays. In the anesthetized guinea pig, QRS widening was also observed but with a higher EC_{20} of 1600 nM. The ≥10-fold window between the EC_{20} and the anticipated free therapeutic C_{max} was deemed sufficient to support progression into further studies aimed at characterizing the in vivo target organ toxicity profile of **UCB7362** at a high dose.

A dose range-finding study was conducted with **UCB7362** at doses of 250, 500, and 1000 mg/kg/every other day in a 7-day oral (gavage) exploratory toxicity study in Han Wistar male rats. The top dose of 1000 mg/kg achieved an AUC integrated total of 2182 μM h (908 μM h AUC free) and a C_{max} total of 25 μM μg/mL (C_{max} free of 11 μM) on day 7, this is 40-fold (AUC integrated total) or 60-fold AUC free and 50-fold (C_{max} total) or 84-fold C_{max} free higher than the anticipated exposure required for clinical efficacy with a 7-dose regimen (Figure 10).

Due to the ability of **UCB7362** to inhibit Cat D, ocular endpoints were added to the study. There were no **UCB7362**-related changes in ophthalmology, auditory reflex, and specific ocular examination (including mydriasis, pupillary reflex, and eye). No toxicologically relevant changes in hematology and clinical pathology parameters were observed. Lower body weight gain was observed throughout the study for the high-dose group animals and, body weight remained lower (−10%) than the control group at the end of the study. This lower body weight gain was associated with a lower food consumption throughout the study.

In the histopathological assessment, following a 7-day dosing period, **UCB7362** induced minimal auto-fluorescent granule (AFG) accumulation in the retinal pigmented epithelium (RPE), which led to minimal hypertrophy of the cells. No changes were observed in the neural part of the retina. No other significant findings were found. AFGs were also observed in the lung and in the mesenteric lymph node suggestive of phospholipidosis.

The observation of minimal AFG accumulation in the RPE is consistent with effects observed for other aspartyl protease inhibitors[55,56] and is likely to be associated with inhibition of the human aspartyl protease, Cat D.[57] Cat D is a major lysosomal enzyme of the RPE cells that is responsible for 80% of the proteolysis of rhodopsin (recycling of photoreceptor). Any undigested residual bodies remain as lipofuscin, a mixture of chemically modified, incompletely digested rod outer segments (ROS) with fluorescent properties. Lipofuscin is not extruded from the cell but slowly accumulates and eventually occupies a considerable part of the cell volume, a well-recognized phenomenon in elderly individuals.[58]

In effect, **UCB7362** was found to be a 3.9 μM inhibitor of Cat D in a biochemical assay (Figure 10). The ability of **UCB7362** to inhibit Cat D was also assessed in a cellular context following the protocol of Zuhl et al.[59] A shift in potency to 36 nM was observed, consistent with the accumulation of the basic molecule into the lysosome. Since reversible, low-severity RPE lipofuscin accumulation is a normal feature of aging with no functional consequences, we sought to ascertain whether the AFG accumulation observed in the high-dose toxicology study had functional consequences, using electroretinography (ERG). An ERG study was carried out following the dosing of **UCB7362** at 1000 mg/kg every other day to measure the electrical response of light-sensitive cells of the eyes under dark (scotopic phase) and light (photopic phase) conditions. Despite the observed minimal morphological changes in the RPE, no effect on ERG

https://doi.org/10.1021/acs.jmedchem.2c01336
J. Med. Chem. 2022, 65, 14121−14143

parameters (scotopic or photopic amplitudes and implicit times/latency) during the dosing period was observed.

Finally, **UCB7362** was assessed for potential genotoxicity and phototoxicity. The embedded aniline was identified as a potential genotoxicity risk for the amide series; thus, both the parent compound and the aniline fragment were tested in micronucleus and microAmes studies. Both compounds showed no signals in either study. **UCB7362** was found to have a minimum extinction coefficient of 2336 L/(mol cm) so the compound was progressed into the 3T3 neutral red uptake model to further understand the phototoxicity risk, but no flag was observed.

3. CONCLUSIONS

Structure-based optimization of a cyclic guanidine core, a well-known motif in the field of aspartyl protease discovery, allowed for the identification of new antimalarial compounds acting through inhibition of Plasmepsin X. This chemotype has demonstrated activity against several stages of the parasite life cycle, supporting PMX as multitarget for antimalarials. The frontrunner compound **3** and **UCB7362** demonstrated in vivo efficacy in murine models of malaria. Despite suboptimal separation between efficacy and safety, the biaryl amine lead compound **3** highlights the potential for this chemical series to deliver potent compounds with long-predicted half-lives in humans that may be compatible with a three-dose or even single dose-cure paradigm for the treatment of uncomplicated malaria.[2] The learnings from this work suggest the importance of incorporating safety evaluation early in the discovery process for PMX inhibitors as antimalarial drugs. **UCB7362**, a structurally differentiated analogue with improved safety profile but shorter predicted human half-life of 14 h, could be progressed toward the development and clinical trials with a potential 7-dose regimen cure for uncomplicated malaria with a daily dose of 50 mg allowing sufficient safety margin. However, due to the current standard of care, a paradigm of 7 doses is considered suboptimal relative to a 3-dose regimen, and therefore, these activities are not being prioritized. Lack of selectivity against Cat D is a concern for aspartyl inhibitors because AFG accumulation can lead to adverse retinal ocular effect.[27] However, studies on **UCB7362** not only showed that the risk of AFG accumulation is monitorable in early in vivo safety studies in rats but also that it is possible to obtain potent PMX inhibitors with sufficient safety margin vs Cat D.

Overall, our work has reinforced the value of PMX as an antimalarial target through the optimization of a druglike chemotype. Further medicinal chemistry efforts focusing on balancing potency, selectivity, and pharmacokinetic parameters may offer the potential to further refine this chemical series and deliver improved clinical candidates that can meet the stringent target candidate profiles[2] defined as high priority for clinical development.

4. EXPERIMENTAL SECTION

4.1. General Synthetic Procedures. Unless otherwise stated, starting materials were purchased from commercially available sources. All reagents were used as received. Commercially available Zn dust was activated by stirring with dilute 1 M HCl, then washing with water, methanol, and acetone, and dried under vacuum at 100−120 °C for 15 min. Reactions involving air- or moisture-sensitive reagents were performed under a nitrogen atmosphere using dried solvents and glassware. Conversion was monitored by thin-layer chromatography (TLC) and liquid chromatography−mass spectrometry (LCMS). ^{1}H and ^{13}C nuclear magnetic resonance (NMR) spectra were recorded on a Bruker ADVANCE 300, 400, or 500 MHz spectrometer at ambient temperature (298 K), and resonances are reported relative to tetramethylsilane. The purities of compounds for biological testing were assessed by NMR and UPLC to be ≥95%. Analytical LCMS method 1. Column: Waters X Bridge C18, 2.1 × 30 mm^2, 2.5 μm; injection volume 5.0 μL; flow rate 1.00 mL/min; detection: MS-ESI$^+$ m/z 150 to 800/UV-DAD 220−400 nm; solvent A 5 mM ammonium formate in water + 0.1% ammonia solvent B acetonitrile + 5% solvent A + 0.1% ammonia; gradient program: 5−95% B in 4.0 min; hold until 5.00 min; at 5.10 min concentration of B is 5%; hold up to 6.5 min.

The human biological samples were sourced ethically, and their research use was in accordance with the terms of the informed consent under an IRB/EC-approved protocol. All animal studies were reviewed and approved prior to start by the institutional ethical committee and/or local competent authority and carried out in accordance with European Directive 2010/63/EEC and the GSK Policy on the Care, Welfare and Treatment of Animals as well as standard operating procedures and/or and institutional policies on the animal care, use, and welfare.

Prophylactic studies in mice were performed at SwissTPH. The animal experiments that were carried out at the Swiss Tropical and Public Health Institute (SwissTPH, Basel, Switzerland) adhered to local and national regulations of laboratory animal welfare in Switzerland (awarded permission no. 2693). Protocols were regularly reviewed and revised following approval by the local authority (Veterinäramt Basel Stadt).

4.1.1. Nomenclature. Compounds were named with the aid of ACD/Name Batch (Network).

*4.1.2. rac-(2S,4S)-2-Methyltetrahydropyran-4-amine (**7**).* To a stirred solution of 2-methyltetrahydropyran-4-one (10.0 g, 87.6 mmol) in MeOH (100 mL) were added benzyl amine (14.3 mL, 131.4 mmol) and acetic acid (0.25 mL, 4.38 mmol) under nitrogen atmosphere and stirred for 4 h at room temperature. Then, $NaCNBH_3$ (8.27 g, 131.4 mmol) was added at RT and stirred for 16 h. The reaction mixture was concentrated under reduced pressure to obtain the crude compound, which was purified by column chromatography (100−200 mesh silica gel and eluted with 30−100% ethyl acetate (EtOAc)/hexane) to afford a pale brown liquid. This was dissolved in MeOH (100 mL), and 10% Pd/C (10.0 g) was added in a Parr shaker vessel, and the reaction was stirred at RT for 16 h. After completion of the reaction, the mixture was passed through a pad of Celite and washed with 10% MeOH/dichloromethane (DCM). The filtrate was concentrated under reduced pressure to obtain the title compound (4.0 g, 71% yield) as a brown liquid. ^{1}H NMR (400 MHz, methanol-d_4) δ 3.95−3.80 (m, 1H), 3.54−3.42 (m, 2H), 2.79−2.68 (m, 1H), 1.95−1.87 (m, 2H), 1.43−1.30 (m, 1H) 1.18 (d, J = 5.87 Hz, 3H), 1.13−1.05 (m, 1H).

*4.1.3. tert-Butyl N-(Tetrahydropyran-4-ylcarbamothioyl)-carbamate (**8**).* To a solution of *N*,*N*′-bis-*tert*-butoxycarbonylthiourea (12.3 g, 44.5 mmol) in THF (100 mL) under nitrogen was added 60% NaH (5 g, 124.5 mmol) portion-wise over a period of 10 min at 0 °C and stirred for 1 h, then TFAA (11.2 mL, 80.1 mmol) was added dropwise at same temperature (0 °C), and stirred for 1 h. A solution of tetrahydropyran-4-amine (4.5 g, 44.5 mmol) in THF (20 mL) was added and stirred at RT for 2 h. After completion, the reaction was quenched with ice-cold water, extracted with EtOAc (2 × 500 mL), and combined organic layers were dried over sodium sulfate. The solvent was evaporated under reduced pressure to get a crude compound, which was purified by column chromatography (silica, 100−200 mesh, 3% ethyl acetate/hexane) to afford the title compound (9.0 g, 77%) as a pale yellow solid. ^{1}H NMR (400 MHz, $CDCl_3$) δ 9.71 (brs, 1H), 7.89 (brs, 1H), 4.54−4.43 (m, 1H), 4.02−3.86 (m, 2H), 3.60−3.52 (m, 2H), 2.14−1.96 (m, 2H), 1.89−1.77 (m, 2H), 1.50 (s, 9H).

*4.1.4. N-[rac-(2S,4S)-2-Methyltetrahydropyran-4-yl]-thioacetamide (**9**).* To a solution of *N*,*N*′-bis-*tert*-butoxycarbonylthiourea (10.3 g, 37.3 mmol) in THF (30 mL) was added NaH (4.48 g, 112 mmol) at 0 °C, and the reaction mixture was stirred at the same

https://doi.org/10.1021/acs.jmedchem.2c01336
J. Med. Chem. 2022, 65, 14121−14143

temperature for 1 h. TFAA (7.89 mL, 56.0 mmol) was added dropwise at 0 °C, and the reaction mixture was stirred at 0 °C for 1 h. A solution of **7** (4.30 g, 37.3 mmol) in THF (5 mL) was added at 0 °C, and the reaction mixture was stirred at room temperature for 4 h. After completion, the reaction mixture was diluted with H_2O (100 mL) and extracted with EtOAc (2 × 50 mL). The organic layer was separated, washed with brine (30 mL), dried over anhydrous Na_2SO_4, and concentrated in vacuo. The crude obtained was purified by column chromatography (silica, 100−200 mesh, 10−20% EtOAc in hexanes) to afford the title compound (4.90 g, 37% yield) as a yellow oil. ^{1}H NMR (400 MHz, $CDCl_3$) δ 9.59 (brd, J = 6.36 Hz, 1H), 7.82 (brs, 1H), 4.47−4.44 (m, 1H), 4.05−3.91 (m, 1H), 3.55−3.45 (m, 2H), 2.10−2.07 (m, 1H), 1.55−1.48 (m, 3H), 1.47 (s, 9H), 1.26−1.21 (m, 3H).

*4.1.5. N-[1-(2-Chloro-3-nitrophenyl)ethylidene]-(R)-2-methylpropane-2-sulfinamide (**11**).* To a solution of 1-(2-chloro-3-nitrophenyl)ethanone (10.5 g, 5.1 mmol) and (*R*)-2-methyl-2-propanesulfinamide (11.2 g, 5.1 mmol) in dry THF (100 mL) was added titanium(IV) ethoxide (23.2 g, 10.5 mmol). The reaction mixture was heated at 75 °C for 12 h, then quenched with H_2O (500 mL), stirred at room temperature for 1 h, and filtered through a pad of Celite. The aqueous layer was extracted with EtOAc (2 × 150 mL). The organic layer was separated and dried over anhydrous sodium sulfate, and then concentrated in vacuo. The crude residue was purified by column chromatography (silica, 100−200 mesh, 30% EtOAc in hexanes) to afford the title compound (10.0 g, 63%) as a red liquid. LCMS (method 1, ESI) 303.00 $[MH]^+$, RT 3.02 min. ^{1}H NMR (400 MHz, dimethyl sulfoxide (DMSO)-d_6, mixture of rotamer) δ 8.81 (d, J = 8.00 Hz, 1H), 7.79 (d, J = 7.20 Hz, 1H), 7.71−7.60 (m, 1H), 2.67 (s, 3H), 1.21 (s, 9H).

*4.1.6. Benzyl N-(3-{N-[(R)-tert-Butylsulfinyl]-C-methyl carbonimidoyl}-2-chlorophenyl)-carbamate (**12**).* To a solution of **11** (10.0 g, 33.2 mmol) in MeOH (100 mL) was added Raney Ni (10.0 g) at room temperature. The reaction mixture was stirred at room temperature for 6 h under an atmosphere of H_2, then filtered through a pad of Celite, and washed with MeOH (150 mL). The filtrate was concentrated in vacuo to afford the title compound (8.80 g, 98%) as a colorless liquid, which was utilized without further purification. This was dissolved in THF (100 mL) and DIPEA (32.5 mL, 183.0 mmol), and then benzyl chloroformate (12.5 g, 73.5 mmol) was added at 0 °C. The reaction mixture was stirred at room temperature for 16 h, then quenched with H_2O (500 mL), and extracted with EtOAc (3 × 250 mL). The organic layer was separated, dried over anhydrous sodium sulfate, and then concentrated in vacuo. The crude residue was purified by column chromatography (silica, 100−200 mesh, 30% EtOAc in *n*-hexanes) to afford the title compound (12.5 g, 84%) as a yellow liquid. LCMS (method 1, ESI) 407.00 $[MH]^+$, RT 3.43 min. ^{1}H NMR (400 MHz, DMSO-d_6, mixture of rotamer) δ 9.34 (s, 1H), 7.63 (d, J = 8.40 Hz, 1H), 7.43−7.30 (m, 6H), 7.23 (d, J = 8.00 Hz, 1H), 5.18 (s, 2H), 2.61 (s, 3H), 1.20 (s, 9H).

*4.1.7. Methyl (3S)-3-Amino-3-[3-(benzyl oxycarbonylamino)-2-chlorophenyl]butanoate (**13**).* A suspension of CuCl (4.37 g, 44.2 mmol) and Zn (14.4 g, 221.0 mmol) in THF (90 mL) was heated at 50 °C for 30 min. Methyl bromoacetate (11.0 g, 66.0 mmol) was added dropwise at 80 °C, and then the reaction mixture was heated at 50 °C for 1 h. Intermediate **12** (9.00 g, 22.0 mmol) was added at 0 °C, and the reaction mixture was stirred at room temperature for 16 h and then filtered through a pad of Celite. The filtrate was washed with brine (300 mL). The organic layer was separated and dried over anhydrous sodium sulfate and then concentrated in vacuo. The crude residue was purified by column chromatography (silica, 100−200 mesh, 40% EtOAc in hexanes) to afford a yellow liquid. This was dissolved in MeOH (80 mL), and 4 M HCl in 1,4-dioxane (15.6 mL, 62.5 mmol) was added at 0 °C. The reaction mixture was stirred at room temperature for 6 h and then concentrated in vacuo. The residue was basified with saturated aqueous $NaHCO_3$ solution (200 mL) and extracted with EtOAc (2 × 250 mL). The organic layer was separated and dried over anhydrous sodium sulfate, and then concentrated in vacuo, to afford the title compound (5.18 g, 90%) as a yellow liquid, which was utilized without further purification. ^{1}H NMR (400 MHz, DMSO-d_6) δ 9.08 (s, 1H), 7.68−7.64 (m, 1H), 7.42−7.25 (m, 7H), 5.10 (s, 2H), 3.75 (s, 2H), 3.48 (s, 3H), 3.25 (d, J = 8.00 Hz, 1H), 2.92 (d, J = 8.4 Hz, 1H), 1.54 (s, 3H).

*4.1.8. tert-Butyl (NE)-N-[(4S)-4-[3(Benzyloxycarbonyl amino)-2-chloro-phenyl]-4-methyl-1-[(2S,4S)-2-methyl tetrahydropyran-4-yl]-6-oxo-hexahydro pyrimidin-2-ylidene]carbamate (**15**).* To a solution of **9** (4.85 g, 13.6 mmol) and **13** (3.94 g, 9.53 mmol) and EDCI (3.90 g, 20.4 mmol) in DMF (15 mL) was added DIPEA (4.75 mL, 27.2 mmol) at 0 °C, and the reaction mixture was stirred at room temperature for 4 h. After completion, the reaction mixture was diluted with ice-cold H_2O (50 mL) and extracted with EtOAc (2 × 20 mL). The organic layer was separated, washed with ice-cold H_2O (2 × 20 mL) and brine (20 mL), dried over anhydrous Na_2SO_4, and concentrated in vacuo to afford a brown oil. This was redissolved in THF (100 mL), and *t*-BuOK (1 M in THF, 10.4 mL, 10.4 mmol) was added at 0 °C, and the reaction mixture was stirred at room temperature for 2 h. The reaction mixture was quenched with H_2O (300 mL) and extracted with EtOAc (2 × 100 mL). The organic layer was separated, dried over anhydrous Na_2SO_4, and concentrated in vacuo. The crude obtained was purified by column chromatography (silica, 100−200 mesh, 25−45% EtOAc in hexanes). The product obtained was repurified by chiral prep high-performance liquid chromatography (HPLC) (method: mobile phase: (A) CO_2 (B) MeOH + methyl *tert*-butyl ether (MTBE) (60:40) + 0.1% iso-propylamine, isocratic: 20% B column: DIACEL CHIRALPAK-IG (250 × 4.6 mm^2, 5 μm), wavelength: 240 nm, flow: 3 mL/min) to afford the title compound (1.60 g, 52%) as an off-white solid. Chiral HPLC purity and retention time: 100% at 8.45 min. LCMS (method 1, ESI) 585.05 $[MH]^+$, RT 2.25 min. ^{1}H NMR (400 MHz, DMSO-d_6) δ 10.52 (s, 1H), 9.26 (brs, 1H), 7.57 (d, J = 11 Hz, 1H), 7.40−7.34 (m, 6H), 7.65 (d, J = 11 Hz, 1H), 5.14 (s, 2H), 4.64−4.63 (m, 1H), 3.84 (dd, J = 11.25, 3.91 Hz, 1H), 3.54−3.48 (m, 1H), 3.26−3.22 (m, 2H), 3.11 (d, J = 16.14 Hz, 1H), 2.38−2.31 (m, 1H), 2.05−1.94 (m, 1H), 1.73 (s, 3H), 1.45 (s, 9H), 1.32 (d, J = 11.74 Hz, 1H), 1.07 (d, J = 11.74 Hz, 1H), 0.99 (d, J = 5.87 Hz, 3H).

*4.1.9. [(4S)-4-(3-Amino-2-chlorophenyl)-4-methyl-1-[(2S,4S)-2-methyltetrahydropyran-4-yl]-6-oxohexa hydropyrimidin-2-ylidene]carbamate (**17**).* To a solution of intermediate **15** (0.83 g, 1.40 mmol) in MeOH (30 mL) was added 20% Pd/C (0.03 g, 0.28 mmol), and the reaction mixture was stirred at room temperature for 3 h under 145 PSI hydrogen pressure. After completion, the reaction mixture was filtered through the pad of Celite, and the filtrate was concentrated in vacuo. The crude obtained was purified by column chromatography (silica, 100−200 mesh, 10−40% EtOAc in hexanes) to afford the title compound (0.41 g, 60%) as an off-white solid. LCMS (method 1, ESI) 451.00 $[MH]^+$, RT 2.03 min. ^{1}H NMR (400 MHz, DMSO-d_6) δ 10.47 (s, 1H), 7.00 (t, J = 7.83 Hz, 1H), 6.78 (d, J = 8.31 Hz, 1H), 6.47 (d, J = 7.83 Hz, 1H), 5.52 (s, 2H), 4.66 (t, J = 11.98 Hz, 1H), 3.76 (dd, J = 11.00, 4.16 Hz, 1H), 3.50 (d, J = 16.14 Hz, 1H), 3.22 (d, J = 11.74 Hz, 1H), 3.11 (d, J = 16.14 Hz, 1H), 2.33−2.23 (m, 1H), 2.07 (d, J = 11.25 Hz, 1H), 1.73 (s, 3H), 1.45 (s, 9H), 1.06 (d, J = 5.87 Hz, 3H), 0.98−0.90 (m, 1H), (2H's merged in solvent peak).

Absolute stereochemistry was determined by VCD spectroscopy with 99% confidence level, as described in the Supporting Information.

*4.1.10. tert-Butyl-N-[(4S)-4-[3-(benzyloxycarbonyl amino)-2-chloro-phenyl]-4-methyl-6-oxo-1-tetra hydropyran-4-yl-hexahydropyrimidin-2-ylidene]carbamate (**14**).* To a solution of **13** (14 g, 33.9 mmol) and **8** (9 g, 33.9 mmol) in DMF (100 mL) were added DIPEA (24 mL, 135.9 mmol) and *N*-(3-dimethylaminopropyl)-*N*′-ethylcarbodiimide hydrochloride (EDC·HCl) (13 g, 67.9 mmol) at 0 °C, and the resulting reaction mixture was stirred at RT for 16 h. After completion, the reaction mixture was diluted with ice-cold water, extracted with EtOAc (2 × 800 mL), and combined organics were washed with brine and dried over sodium sulfate. The solvent was evaporated under reduced pressure to get a crude compound, which was purified by column chromatography. This was dissolved in THF (100 mL), and potassium *tert*-butoxide in THF 1 M (29.8 mL, 29.8 mmol) was added under nitrogen at 0 °C over a period of 10 min.

https://doi.org/10.1021/acs.jmedchem.2c01336
J. Med. Chem. 2022, 65, 14121−14143

The reaction mixture was stirred at RT for 45 min and then quenched with ammonium chloride solution and extracted with EtOAc (2 × 800 mL). The combined organics were washed with brine and dried over sodium sulfate. The solvent was evaporated under reduced pressure to get crude compound, which was purified by column chromatography (silica gel, 100−200, 30% EtOA/hexane) to afford the title compound (7.5 g, yield 88%) as an off-white solid. LCMS (method 1, ESI) 2.21 min; 571.75 $[MH]^+$. ^{1}H NMR (400 MHz, $CDCl_3$) δ 10.58 (brs, 1H), 8.19 (d, J = 7.83 Hz, 1H), 7.45−7.35 (m, 8H), 7.04−7.02 (m, 1H), 5.22 (s, 2H), 4.81−4.73 (m, 1H), 3.96 (dd, J = 11.74, 4.40 Hz, 1H), 3.89 (dd, J = 11.25, 4.40 Hz, 1H), 3.65 (dd, J = 16.14, 1.47 Hz, 1H), 3.45−3.38 (m, 1H), 3.36−3.29 (m, 1H), 2.83 (d, J = 16.14 Hz, 1H), 2.66−2.60 (m, 1H), 2.55−2.51 (m, 1H), 1.82 (s, 3H), 1.54 (s, 9H), 1.51−1.44 (m, 1H), 1.12−1.02 (m, 1H).

*4.1.11. tert-Butyl N-[(4S)-4-(3-Amino-2-chloro-phenyl)-4-methyl-6-oxo-1-tetrahydropyran-4-yl-hexahydro pyrimidin-2-ylidene]-carbamate (**16**).* To a solution of **14** (8.0 g, 14.0 mmol) in MeOH (100 mL) was added 10% Pd/C (800 mg), and the reaction mixture was stirred under hydrogen balloon pressure at RT for 30 min. After completion, the reaction mixture was filtered through Celite and washed with methanol. The filtrate was concentrated under reduced pressure to afford a crude compound, which was purified by column chromatography (silica gel, 100−200, 30% EtOAc/hexane) to afford the title compound (5.5 g, 89%) as an off-white solid. LCMS (method 1, ESI) 2.08 min; 437.20 $[MH]^+$. ^{1}H NMR (400 MHz, $CDCl_3$) δ 10.53 (brs, 1 H), 7.05−6.99 (m, 1H), 6.75 (d, J = 7.82 Hz, 1H), 6.68 (d, J = 7.83 Hz, 1H), 4.85−4.74 (m, 1H), 4.20 (brs, 2H), 3.97 (dd, J = 11.25, 4.40 Hz, 1H), 3.90 (dd, J = 11.25, 4.40 Hz, 1H), 3.67 (dd, J = 16.14, 1.47 Hz, 1H), 3.48−3.42 (m, 1H), 3.39−3.31 (m, 1H), 2.81 (d, J = 16.63 Hz, 1H), 2.68−2.62 (m, 1H), 2.58−2.53 (m, 1H), 1.84 (s, 3H), 1.54 (s, 9H), 1.50−1.47 (m, 1H), 1.13−1.09 (m, 1H).

*4.1.12. (6S)-6-(3-Anilino-2-chloro-phenyl)-2-imino-6-methyl-3-tetrahydropyran-4-yl-hexahydro pyrimidin-4-one·TFA (**1**).* To a solution of **16** (0.50 g, 1.14 mmol) in DCM (20 mL) were added phenyl boronic acid (0.56 g, 4.58 mmol), $Cu(OAc)_2$ (1.04 g, 5.72 mmol), and TEA (0.96 mL, 6.87 mmol) at room temperature. The reaction mixture was stirred at room temperature for 16 h under an oxygen atmosphere. After completion, the reaction mixture was quenched with H_2O (200 mL) and extracted with EtOAc (2 × 150 mL). The organic layer was separated, dried over anhydrous Na_2SO_4, and concentrated in vacuo. The crude obtained was purified by column chromatography (silica, 100−200 mesh, 15−35% EtOAc in hexanes) as an off-white solid, to which was added TFA (1.57 g, 13.8 mmol) in DCM (6 mL) at 0 °C. The reaction mixture was stirred at room temperature for 3 h. Progress of the reaction mixture was monitored by TLC and LCMS. After completion, the reaction mixture was concentrated in vacuo. The crude obtained was purified by prep HPLC (TFA as a solvent system) to afford the title compound (0.285 g, 78%) as a TFA salt and an off-white solid. LCMS (method 1, ESI) 413.00 $[MH]^+$, RT 2.50 min. High-resolution mass spectrometry (HRMS) (time-of-flight mass spectrometry (TOF MS) ES+) calcd for $C_{22}H_{26}N_4O_2Cl$ (MH^+) 413.1744 measured 413.1749. ^{1}H NMR (400 MHz, DMSO-d_6) δ ^{1}H NMR (400 MHz, DMSO-d_6) δ 10.64 (s, 1H), 8.88 (brs, 2H), 7.75 (s, 1H), 7.29−7.23 (m, 2H), 7.20−7.17 (m, 2H), 7.06 (d, J = 7.83 Hz, 2H), 6.93 (t, J = 7.34 Hz, 1H), 6.85 (dd, J = 6.36, 2.93 Hz, 1H), 3.90−3.82 (m, 2H), 3.78−3.73 (m, 1H), 3.71−3.67 (m, 1H), 3.32−3.25 (m, 2H), 3.13 (t, J = 11.00 Hz, 1H), 2.39−2.30 (m, 1H), 2.23−2.13 (m, 1H), 1.77 (s, 3H), 1.66 (d, J = 11.74 Hz, 1H), 0.81 (d, J = 11.74 Hz, 1H).

*4.1.13. (6S)-6-[2-Chloro-3-[(6-cyclopropyl-3-pyridyl)amino]-phenyl]-2-imino-6-methyl-3-tetrahydropyran-4-yl-hexahydropyrimidin-4-one·HCl (**2**).* To a mixture of **16** (60.3 g, 138 mmol) were added 5-bromo-2-cyclopropyl-pyridine (35.5 g, 179 mmol), 2-(dicyclohexylphosphino)3,6-dimethoxy-2′,4′,6′-triisopropyl-1,1′-biphenyl (15.4 g, 27.5 mmol), Brettphos Pd G3 (13.2 g, 13.8 mmol), and sodium *tert*-butoxide (46.5 g, 483 mmol) under nitrogen was added anhydrous 1,4-dioxane (550 mL). The mixture was mechanically stirred at ambient temperature for 15 min and then heated to 60 °C for 1.5 h before being cooled to ambient temperature and aged for 17 h. Saturated ammonium chloride solution (500 mL) and H_2O (200 mL) and AcOEt (900 mL) were added. The aqueous layer was extracted with AcOEt (600 mL). The combined organics were concentrated under reduced pressure, and the residue was purified by flash chromatography (silica, 0−80% ethyl acetate in isohexane). After concentration under reduced pressure, the residue was dissolved in AcOEt (700 mL) and slurried with KP-NH silica (165 g). The silica was filtered off, and the cake was washed with ethyl acetate. The organics were concentrated under reduced pressure to afford the desired product as a beige foam. To this was added HCl (4 mol/L) in 1,2-dioxane (500 mL) followed by DCM (400 mL). After 2.5 h, the mixture was concentrated under reduced pressure to give a foam. The foam was dissolved in water (200 mL) and concentrated under reduced pressure to give the title compound as a yellow powder (64.0 g, 100%). LCMS (method 1, ESI) 1.54 min; 454.2 $[MH]^+$. HRMS (TOF MS ES+) calcd for $C_{24}H_{29}N_5O_2Cl$ (MH^+) 454.2010 measured 454.2013. ^{1}H NMR (300 MHz, DMSO-d_6) δ 10.99 (s, 1H), 9.48 (s, 1H), 9.24 (s, 1H), 8.98 (s, 1H), 8.11 (d, J = 2.6 Hz, 1H), 7.90 (dd, J = 9.0, 2.6 Hz, 1H), 7.51 (d, J = 9.1 Hz, 1H), 7.47−7.29 (m, 2H), 7.15 (dd, J = 7.6, 1.8 Hz, 1H), 4.18−3.96 (m, 1H), 3.88−3.78 (m, 1H), 3.79−3.63 (m, 2H), 3.49−3.30 (m, 2H), 3.25−3.09 (m, 1H), 2.47−2.24 (m, 2H), 2.15 (qd, J = 12.0, 4.6 Hz, 1H), 1.79 (s, 3H), 1.76−1.62 (m, 1H), 1.27−1.06 (m, 4H), 0.90 (d, J = 12.0 Hz, 1H). ^{13}C NMR (101 MHz, DMSO) δ 168.0, 155.7, 150.5, 140.5, 140.4, 139.8, 132.4, 128.4, 123.6, 123.4, 122.3, 121.7, 67.1, 66.9, 56.1, 55.5, 43.72, 29.3, 29.0, 25.4, 13.8, 11.0.

*4.1.14. (6S)-6-[2-Chloro-3-[(6-cyclopropyl-3-pyridyl)amino]-phenyl]-2-imino-6-methyl-3-[(2S,4S)-2-methyltetrahydropyran-4-yl]hexahydropyrimidin-4-one·HCl (**3**).* To a nitrogen-purged mixture of **17** (32.6 g, 72 mmol), 5-bromo-2-cyclopropyl-pyridine (19.0 g, 95.9 mmol), sodium *tert*-butoxide (23.7 g, 247 mmol), BrettPhos (8.1 g, 14 mmol), and BrettPhos Pd G3 (6.9 g, 7.2 mmol) was added anhydrous 1,4-dioxane (290 mL). The reaction was heated at RT under an inert atmosphere for 1 h and then warmed to 60 °C and stirred for an additional 2 h. Saturated ammonium chloride (200 mL), water (200 mL), and *tert*-butyl methyl ether (TBME) (250 mL) were added. The aqueous solution was extracted with TBME (2 × 300 mL), and the combined organics were dried over sodium sulfate and then concentrated. The resulting material was purified by flash chromatography (gradient elution 0−70% ethyl acetate/isohexane). Clean fractions were combined and concentrated to give a pale yellow foam. This was dissolved in AcOEt (200 mL), and Biotage KP-NH silica (90 g) was added. The suspension was stirred for 10 min, and then the silica was filtered off and washed with AcOEt until no remaining product eluted. The solvent was removed to afford the title compound as a pale yellow foam. This was dissolved in DCM (250 mL), and 4 M HCl in 1,4-dioxane (175 mL) was added and stirred at room temperature for 1 h. The reaction mixture was concentrated under reduced pressure, then dissolved in 1% HCl solution (300 mL), and extracted with diethyl ether (2 × 200 mL). The aqueous solution was concentrated under reduced pressure to afford a pale solid. This was redissolved in 2.5% HCl in water (750 mL). Methanol (40 mL) and DCM (400 mL) were added, and the mixture was vigorously stirred, then separated, and the aqueous was washed with DCM (2 × 300 mL). The aqueous solution was concentrated under reduced pressure and dried to afford the title compound as the HCl salt (38.03 g, 95.0%). LCMS (method 1, ESI) 468.00 $[MH]^+$, RT 1.78 min. HRMS (TOF MS ES+) calcd for $C_{25}H_{31}N_5O_2Cl$ (MH^+) 468.2166 measured 468.2169. ^{1}H NMR (400 MHz, in DMSO-d_6) δ 10.74 (brs, 1H), 9.01 (brs, 2H), 8.55 (brs, 1H), 8.15−8.06 (m, 1H), 7.74 (d, J = 7.34 Hz, 1H), 7.40 (d, J = 8.80 Hz, 1H), 7.30 (s, 2H), 7.04−7.02 (m, 1H), 3.93−3.87 (m, 1H), 3.75−3.62 (m, 2H), 3.41−3.36 (m, 2H), 3.29 (d, J = 16.14 Hz, 1H), 3.17 (t, J = 11.25 Hz, 1H), 2.26−2.23 (m, 1H), 2.08−2.02 (m, 1H), 1.98−1.94 (m, 1H), 1.75 (s, 3H), 1.14−1.12 (m, 2H), 1.04 (d, J = 5.87 Hz, 3H), 1.02−0.99 (m, 2H), 0.82 (d, J = 10.76 Hz, 1H). ^{13}C NMR (126 MHz, DMSO-d_6) δ 168.00, 155.8, 150.4, 140.6, 140.4, 139.8, 132.9, 128.4, 123.7, 123.4, 122.3, 121.8, 72.7, 66.4, 56.2, 55.5, 43.7, 36.0, 28.5, 25.4, 21.9, 13.8, 11.0.

*4.1.15. (6S)-6-[2-Chloro-3-[(2-cyclopropylpyrimidin-5-yl)amino]-phenyl]-2-imino-6-methyl-3-[(2R,4R)-2-methyltetrahydropyran-4-yl]hexahydropyrimidin-4-one;hydrochloride,HCl (**4**).* To a nitrogen-

https://doi.org/10.1021/acs.jmedchem.2c01336
J. Med. Chem. 2022, 65, 14121−14143

purged mixture of compound **17** (36.8 g, 82 mmol), 5-bromo-2-cyclopropylpyrimidine (22 g, 110 mmol) sodium *tert*-butoxide (28 g, 282 mmol), 2-(dicyclohexylphosphino)3,6-dimethoxy-2′,4′,6′-triisopropyl-1,1′-biphenyl (9.1 g, 16 mmol), and Brettphos Pd G3 (7.8 g, 8.2 mmol) was added anhydrous 1,4-dioxane (330 mL). The mixture was stirred at ambient temperature for 2 h and then heated to 50 °C for 20 h. Dichloromethane (200 mL) was added followed by saturated ammonium chloride solution (300 mL). The aqueous phase was extracted with DCM (2 × 200 mL). The organics were passed through a hydrophobic frit and concentrated under reduced pressure. The residue was purified by flash chromatography (silica, 0−80% AcOEt in isohexane). After concentration under reduced pressure, the residue was dissolved in AcOEt (350 mL) and slurried with KP-NH silica (80 g). The silica was filtered off, and the cake was washed with ethyl acetate. The process was repeated twice. The organics were concentrated under reduced pressure to afford the title compound as a pale yellow foam. It was dissolved in DCM (380 mL), and TFA (60 mL, 770 mmol) was added. After 4.5 h, the mixture was concentrated under reduced pressure. The residue was taken up in DCM (500 mL) and saturated sodium bicarbonate solution (500 mL). Sodium bicarbonate was added until pH 7 was obtained. The organics were then washed with saturated sodium bicarbonate solution (400 mL), brine (400 mL), water (500 mL), and saturated sodium bicarbonate solution (300 mL). After concentration under reduced pressure, the residue was dissolved in AcOEt (500 mL) and washed with 5% ammonia solution (2 × 250 mL) and water (250 mL). The organics were dried over sodium sulfate and then concentrated under reduced pressure. To the residue were added 1,4-dioxane (250 mL) and 4 M HCl in 1,4-dioxane (36 mL). Water (200 mL) was added, and the mixture was concentrated under reduced pressure. Additional water (200 mL) was added, and the mixture was concentrated under reduced pressure to ensure all 1,4-dioxane was removed. After drying, the title compound was obtained as a yellow solid (36.2 g, 88%). LCMS (method 1, ESI) 469.2 $[MH]^+$, RT 1.78 min. ^{1}H NMR (300 MHz, DMSO-d_6) δ 10.69 (s, 1H), 8.97 (s, 2H), 8.43 (s, 2H), 8.03 (s, 1H), 7.26−7.18 (m, 1H), 7.14 (dd, J = 8.2, 1.5 Hz, 1H), 6.92 (dd, J = 7.8, 1.6 Hz, 1H), 3.99−3.82 (m, 1H), 3.79−3.62 (m, 2H), 3.50−3.35 (m, 1H), 3.30 (d, J = 16.5 Hz, 1H), 3.19 (t, J = 11.7 Hz, 1H), 2.22−1.91 (m, 3H), 1.78 (s, 3H), 1.76−1.68 (m, 1H), 1.07 (d, J = 6.1 Hz, 3H), 1.04−0.90 (m, 4H), 0.88−0.78 (m, 1H).

*4.1.16. (S)-N-(2-Chloro-3-(2-imino-4-methyl-6-oxo-1-(tetrahydro-2H-pyran-4-yl)hexahydropyrimidin-4-yl)phenyl)benzamide·TFA (**5**).* To a solution of **16** (0.10 g, 0.22 mmol) in DCM (7 mL) was added pyridine (0.04 mL, 0.45 mmol) at 0 °C followed by addition of benzoyl chloride (0.04 g, 0.27 mmol). The reaction mixture was stirred at room temperature for 2 h. After completion, the reaction mixture was quenched with H_2O (20 mL) and extracted with EtOAc (2 × 25 mL). The organic layer was separated, dried over anhydrous Na_2SO_4, and concentrated *in vacuo*. The resulting material was purified by flash chromatography (gradient elution 0−30% ethyl acetate/isohexane) to afford *tert*-butyl (*S*,*E*)-(4-(3-benzamido-2-chlorophenyl)-4-methyl-6-oxo-1-(tetrahydro-2*H*-pyran-4-yl)-tetrahydropyrimidin-2(1*H*)-ylidene)carbamate (0.10 g, 81%) as an off-white solid. This was dissolved in DCM (10 mL) and added with TFA (0.41 g, 3.60 mmol) at 0 °C, and the reaction mixture was stirred at room temperature for 6 h. After completion, the reaction mixture was concentrated *in vacuo*. The crude obtained was purified by washing with Et_2O (5 mL), hexane (10 mL), and lyophilized with CH_3CN/H_2O (5 mL) to afford the title compound as a TFA salt and an off-white solid (0.095 g, 94%). LCMS (method 1, ESI) 441.00 $[MH]^+$, RT 2.1 min. HRMS (TOF MS ES+) calcd for $C_{23}H_{26}N_4O_3Cl$ (MH^+) 441.1693 measured 441.1703. ^{1}H NMR (400 MHz, in DMSO-d_6) δ 10.73 (brs, 1H), 10.10 (s, 1H), 8.96 (brs, 2H) 8.01−7.96 (m, 2H), 7.63−7.59 (m, 2H), 7.56−7.51 (m, 2H), 7.43 (t, J = 8.07 Hz, 1H), 7.31 (d, J = 7.82 Hz, 1H), 3.94−3.82 (m, 2H), 3.80−3.68 (m, 2H), 3.31−3.26 (m, 1H), 3.13 (t, J = 11.25 Hz, 1H), 2.41−2.34 (m, 1H), 2.21−2.12 (m, 1H), 1.78 (s, 3H), 1.72−1.63 (m, 1H), 0.82−0.79 (m, 1H), (1H merged in solvent peak). ^{13}C NMR (101 MHz, DMSO) δ 168.28, 165.88, 159.9 (q, J = 31.6 Hz, CF_3), 155.43, 138.99, 137.75, 134.23, 132.44, 129.51, 129.02, 128.26, 128.15, 127.61, 125.31, 67.12, 66.94, 56.10, 55.71, 43.96, 29.26, 29.05, 25.37.

*4.1.17. N-[2-Chloro-3-[(4S)-2-imino-4-methyl-1-[(2S,4S)-2-methyltetrahydropyran-4-yl]-6-oxohexahydro pyrimidin-4-yl]phenyl]-3-cyano-benzamide·HCl (**UCB7362**).* To a suspension of 3-cyanobenzoic acid (20.4 g, 136 mmol) in DCM (160 mL) at 0 °C was added oxalyl chloride (18 mL). After 10 min, a few drops of DMF were added and the reaction was warmed to ambient temperature and stirred for 2 h. The solvent was removed to afford the acid chloride as an off-white crystalline solid obtained. To a solution of **17** (45 g, 90.80 mmol) and pyridine (22 mL, 272 mmol, 100 mass %) in DCM (450 mL) at 0 °C was added a solution of the acid chloride (18.7 g, 111 mmol) in DCM (120 mL). After 1.5 h, the reaction was complete, so the mixture was washed with water (200 mL) and the organics passed through a hydrophobic frit and concentrated. The residue was taken up in toluene (300 mL) and reevaporated to remove residual pyridine (the process was repeated three times). The oil was dissolved in DCM, filtered through a frit to remove the precipitate, and the filtrate was purified by flash chromatography (0−60% ethyl acetate in isohexane). The resulting product was dissolved in ethyl acetate (400 mL) and KP-NH silica (50 g) was added. The slurry was filtered through a sinter and washed with ethyl acetate until the desired compound ceased to elute and the solvent was removed to afford a white solid. This was dissolved in 1,4-dioxane (460 mL) and DCM (140 mL) and cooled to 0 °C (internal temp 3−4 °C). 4 M HCl in dioxane (230 mL) was then added and the mixture was allowed to warm to ambient temperature and stirred overnight. Additional 4 M HCl in dioxane (20 mL) was added, and the reaction was stirred for a further 2 h. The reaction mixture was concentrated under reduced pressure at 20 °C. The product was dissolved in DCM (500 mL) and washed with saturated bicarb solution (500 mL). The organic layer was washed with water (500 mL). The aqueous phase was back-extracted with DCM (500 mL). Organics were passed through a hydrophobic frit and concentrated to give a foam. This was dissolved in DCM and purified by flash chromatography. (KP-NH columns, gradient from 0 to 5% methanol in DCM) to isolate the free base. This was dissolved in DCM (∼300 mL), and 2 M HCl in Et_2O (2 equiv.) was added. The mixture was then concentrated under reduced pressure and dried to give the title compound (38.6 g, 80.3%) LCMS (method 1, ESI) 480.00 $[MH]^+$, RT 2.1 min. HRMS (TOF MS ES+) calcd for $C_{25}H_{27}N_5O_3Cl$ (MH^+) 480.1802 measured 480.1803. ^{1}H NMR (400 MHz, DMSO-d_6) δ 10.77 (s, 1H), 10.40 (s, 1H), 9.04 (s, 2H), 8.51−8.39 (m, 1H), 8.39−8.19 (m, 1H), 8.22−8.06 (m, 1H), 7.90−7.72 (m, 1H), 7.61 (dd, J = 7.9, 1.5 Hz, 1H), 7.54−7.42 (m, 1H), 7.35 (dd, J = 8.0, 1.6 Hz, 1H), 4.05−3.87 (m, 1H), 3.83−3.63 (m, 2H), 3.57−3.30 (m, 2H), 3.20 (td, J = 12.0, 2.1 Hz, 1H), 2.20−1.91 (m, 2H), 1.81 (s, 3H), 1.76 (d, J = 11.7 Hz, 1H), 1.08 (d, J = 6.1 Hz, 3H), 0.84 (d, J = 12.1 Hz, 1H). ^{13}C NMR (126 MHz, DMSO) δ 167.9, 164.2, 155.8, 139.1, 137.3, 135.8, 135.3, 132.9, 131.9, 130.5, 129.6, 128.2, 127.7, 125.6, 118.7, 112.2, 72.8, 66.4, 56.2, 55.6, 43.7, 36.0, 28.6, 25.5, 21.8.

4.2. Expression and Purification of Recombinant *Pf*PMX (R28p-N573) in HEK Cells. The synthetic gene encoding the *Pf*PMX (R28p-N573) of *P. falciparum* plasmepsin X (XP_001349441) (Figure 2) was engineered for expression in a mammalian host by GeneArt (Thermo Fisher, Waltham, MA) and cloned into a variant of pTT5 with the mouse Ig secretion signal peptide on the N terminus and a tobacco etch virus (TEV)-cleavable 8× Histidine tag on the C-terminus. The recombinant protein was expressed in Expi293F GnTI- cells (Thermo Fisher, Waltham, MA) at 37 °C, using Expi293 expression media (Thermo Fisher, Waltham, MA). After 5 days of culture, the medium was clarified by centrifugation, filtered, and applied to 2 × 5 mL HisTrap Ni Excel columns equilibrated with buffer A (25 mM Tris−HCl, pH 8.0, 200 mM NaCl, 1 mM tris(2-carboxyethyl)phosphine (TCEP), 50 mM arginine, 0.25% glycerol). After the protein was loaded, the column was washed with 50 mL of 2% buffer B (25 mM Tris−HCl, pH 8.0, 200 mM NaCl, 1 mM TCEP, 500 mM imidazole), followed by 50 mL of 4% buffer B. The protein was eluted with a linear gradient of 4−60% buffer B. Fractions were analyzed by sodium dodecyl sulfate-

https://doi.org/10.1021/acs.jmedchem.2c01336
J. Med. Chem. 2022, 65, 14121−14143

polyacrylamide gel electrophoresis (SDS-PAGE) using 4−12% gradient gels in 3-(*N*-morpholino)propanesulfonic acid (MOPS) buffer. Fractions containing the *Pf*PMX were pooled, and 70 mg of TEV protease and 17 mg of EndoH were added and dialyzed overnight at room temperature into buffer A. The extent of tag removal and deglycosylation was assessed by SDS-PAGE. The untagged and deglycosylated protein was applied to 1× 5 mL HiTrap Ni chelating column equilibrated with buffer A. The column was washed 50 mL of buffer A, and the protein was eluted with a linear gradient of 0−60% buffer B. Fractions containing the untagged and deglycosylated *Pf*PMX were observed in the flow through and fractions 1−3 of the gradient elution. The fractions were pooled and dialyzed overnight at 4 °C into size exclusion chromatography (SEC) buffer (50 mM 2-(*N*-morpholino)ethanesulfonic acid (MES), pH 5.5, 200 mM NaCl, 1 mM TCEP, 509 mM arginine, 0.25% glycerol) and then concentrated to 14.3 mg/mL for size exclusion chromatography (SEC). The concentrated protein was applied to a 1 × 120 mL Superdex 200 column in SEC buffer. Fractions containing the protein of interest were pooled and concentrated to 10.29 mg/mL for crystallization. A portion of the pro-domain, residues R27−F135, remains bound to the protein throughout the purification.

4.3. Crystallization and Structure Solution of *Pf*PMX with Compound 4. The protein was co-crystallized with compound **4** by mixing *Pf*PMX at 10.29 mg/mL (160 mM) with 1 mM compound and incubating at 25 °C for 60 min. After incubation, crystallization was carried out in sitting drop trays set up as 0.1 mL protein + compound plus 0.1 mL well solution. The trays were held at 14 °C. After 14 days, crystals were observed in the MCSG-1 screen, condition A4 (0.2 M $MgCl_2$, 0.1 M Na_3Citrate, pH 5.5, 40% (w/v) poly(ethylene glycol) (PEG) 400). (Per PDB file header: Rigaku Reagents JCSG+ A7, optimized,100 mM Tris−HCl/NaOH pH 9.4, 17.86% (w/v) PEG 8000.) The crystals were cryoprotected with 20% ethylene glycol and vitrified in liquid nitrogen. Diffraction data to 2.85 Å resolution were collected at Beamline 21-ID-F at the Advanced Photon Source, Argonne IL on a Rayonix MX-300 CCD detector.

The structure was solved via Molecular Replacement with PHASER[60] using the apo *Pf*PMX structure,[17] PDB code 7RY7, after removing the pre-domain (residues 23−129). The structure was further modeled in iterative cycles of real space refinement in Coot[61] and through reciprocal space refinement in PHENIX.[62] The data collection and refinement statistics are presented in the Supporting Information (Table S2). Quality assessment tools built into COOT, PHENIX, and Molprobity[63] were used to assess the quality of the structure during refinement.

4.4. 3D7 *Pf*-LDH Asexual Blood Stage Assay. *P. falciparum* 3D7 (from BEI resource) lactate dehydrogenase (*Pf*-LDH) growth inhibition assay was carried out as described by Gamo et al.[19] with minor modification in the culture state of inoculum (10−15% parasitemia with ≥80% rings).

Data were normalized to percent growth inhibition with respect to positive (0.2% DMSO as 0% inhibition) and negative (mixture of 100 mM chloroquine and 100 mM atovaquone as 100% inhibition) controls.

Assay acceptance criteria: $Z' > 0.5$; signal/background ratio: 4−6; atovaquone IC_{50} 0.25−2.5 nM, chloroquine IC_{50} 130−260 nM.

4.5. In Vitro Selection Studies for Resistance Profiling. *4.5.1. Drug Preparation.* Drug stocks were made at 10 and 1 mM in dimethyl sulfoxide (DMSO). Aliquots in use were stored at −20 °C and long-term storage was at −80 °C. All in vitro studies were performed such that the final DMSO concentration was <0.5%.

4.5.2. Parasite Culture. *P. falciparum* asexual blood stage parasites were cultured at 3% hematocrit in human O+ red blood cells in Roswell Park Memorial Institute (RPMI)-1640 media, supplemented with 25 mM 4-(2-hydroxyethyl)-1-piperazineethanesulfonic acid (HEPES), 50 mg/L hypoxanthine, 2 mM L-glutamine, 0.21% sodium bicarbonate, 0.5% (w/v) AlbuMAXII (Invitrogen), and 10 μg/mL gentamycin, in modular incubator chambers (Billups-Rothenberg) gassed with a 5% O_2, 5% CO_2, and 90% N_2 mixture and maintained at 37 °C. Dd2 parasites were obtained from T. Wellems (NIAID, NIH). Dd2-B2 is a genetically homogeneous line that was cloned from Dd2 by limiting dilution in the Fidock lab.

4.5.3. Drug Susceptibility Assays (Compound 3). To define the IC_{50} and IC_{90} of ABS parasites, we exposed Dd2-B2 ring-stage cultures at 0.3% parasitemia and 1% hematocrit for 72 h to a range of 10 drug concentrations that were 2-fold serially diluted in duplicates along with drug-free controls. Parasite survival was assessed by flow cytometry on an iQue flow cytometer (Sartorius) using SYBR Green and MitoTracker Deep Red FM (Life Technologies) as nuclear stain and vital dyes, respectively.

Inocula of 2×10^5 parasites were plated as 24 replicates in a 96-well plate so as to calculate the minimum inoculum of resistance value if it fell in the range of 2×10^5 to 4.8×10^6 parasites. The selection was set up at 0.4% parasitemia and 2% hematocrit in 200 μL volumes per well. Due to the small size and number of replicates, the selection was monitored daily for complete killing by measuring percent parasitemia via flow cytometry. Once the populations had fallen below 0.09%, they were noted as clear because, at this low level, the culture would appear clear when performing a thin blood smear (the normal method for monitoring cultures during selections). Once clear, fresh drug media was added to the cultures twice a week. The cultures were passaged once a week by replacing a third of the culture with media and fresh red blood cells. Wells were then monitored twice a week over 60 days by flow cytometry to screen for parasite recrudescence.

2×10^7 Parasite selections were performed in triplicate in 3 mL cultures at 2% parasitemia and 4% hematocrit. The wells were monitored daily for complete killing by blood smears until the culture was clear of parasites. Drug-containing media was replaced daily until the culture was clear of parasites and then every other day thereafter. The cultures were passaged once a week by replacing a fourth of the culture with media and fresh red blood cells. They were monitored twice a week over 60 days by blood smears for signs.

*4.5.4. Drug Susceptibility Assays (**UCB7362**).* To define the IC_{50} and IC_{90} of asexual blood stage parasites, we exposed ring-stage cultures at 0.2% parasitemia and 1% hematocrit to a range of 10 drug concentrations that were 2-fold serially diluted in duplicates, along with drug-free controls. Parasite lines included the drug-sensitive parental line Dd2-B2 and the drug-pressured resistant lines. Parasite survival was assessed by flow cytometry on an iQue Plus (Sartorius) using SYBR Green and MitoTracker Deep Red FM (Life Technologies) as nuclear stain and vital dyes, respectively. IC_{50} and IC_{90} values were derived by nonlinear regression analysis of the percent inhibition data[64]

4.5.5. Whole-Genome Sequence Analysis. The Dd2B2 parent and compound **3** and **UCB7632**-resistant clones were subjected to whole-genome sequencing using an Illumina TruSeq DNA polymerase chain reaction (PCR)—free library preparation protocol and a MiSeq sequencing platform, as previously described. Additional information can be found in the Supporting Information.[65]

4.6. In Vitro Parasite Reduction Ratio (PRR) Assay. The in vitro parasite rate reduction (PRR) assay was conducted as previously described.[47] Briefly, 0.5% parasitemia 3D7 (BEI Resources) *P. falciparum* parasites (≥80% ring-stage population) at 2% hematocrit were exposed to compounds for 120 h at a concentration corresponding to 10 × EC_{50}. Drug was renewed daily over the entire treatment period. Samples of parasites were taken from the treated culture at intervals (24, 48, 72, 96, and 120 h time points), the drug was washed out, and drug-free parasites were cultured in 96-well plates by adding fresh erythrocytes and new culture media. The number of viable parasites was determined by the serial dilution technique. Four independent serial dilutions were done with each sample to correct for experimental variation.

4.7. *Pf*-Resistant Laboratory Strains and Cross-Resistance. The testing was performed with the modified [^{3}H]-hypoxanthine incorporation assay, as previously reported.[32]

4.8. In Vivo Efficacy Studies Using *P. falciparum* Severe Combined Immunodeficient (SCID) Mouse Model. Therapeutic efficacy studies in mice were performed at TAD as previously described with minor modifications.[66] The studies were approved by The Art of Discovery Institutional Animal Care and Use Committee

https://doi.org/10.1021/acs.jmedchem.2c01336
J. Med. Chem. 2022, 65, 14121−14143

(TAD-IACUC), certified by the Biscay County Government (Bizkaiko Foru Aldundia, Basque Country, Spain) to evaluate animal research projects from Spanish institutions according to point 43.3 from Royal Decree 53/2013, from the 1st of February (BOE-A-2013-1337). All experiments were carried out in accordance with European Directive 2010/63/EU. The results from the animal experiments were reported following ARRIVE guidelines (https://www.nc3rs.org.uk/arrive-guidelines) except for disclosure of business trade confidential information. The human biological samples were sourced ethically, and their research use was in accordance with the terms of the informed consent.

The experiments were performed using 22−28 g female NOD-scid IL-2Rγnull mice (NSG) (Charles River, France) adapted to TAD facilities for at least 1 week before entering experimental procedures. The mice were housed in The Art of Discovery animal facility at BIC Bizkaia building (Derio, Basque Country, Spain), which is equipped with high efficiency particulate air (HEPA) filtered in/out air-conditioned with 15 air renovations per hour at 22 ± 2 °C; 40−70% relative humidity; 12 h light/dark period. The mice were accommodated in racks with ventilated disposable cages (Innovive) in groups of up to five individuals with autoclaved dust-free corncob bedding (Innovive). The mice were fed ad libitum with γ-irradiated standard pellet (Envigo) and ultrafiltered water (Innovive) ad libitum.

Prior to infection with *P. falciparum* Pf3D70087/N9,[67] immunodeficient NSG mice were engrafted with human erythrocytes to have a minimum of 40% of human erythrocytes circulating in peripheral blood during the whole experiment. To achieve this, each mouse was inoculated with 50−75% hematocrit erythrocyte suspensions (Basque Center of Transfusion and Human Tissues, Galdakao, Spain, Centro de Transfusiones de la Comunidad de Castilla y León, Valladolid, Spain and Bank of Blood and Tissues, Barcelona, Spain) in RPMI-1640 medium, 25% (v/v) decomplemented human serum, 3.1 mM hypoxanthine by intraperitoneal (IP) and/or intravenous (IV, via tail lateral vein) route. The injection volumes were 1 and 0.7 mL for IP or IV inoculation, respectively.

Engrafted NSG mice were infected with 0.3 mL of an erythrocyte suspension containing 1.17×10^8 parasitized erythrocytes per mL from peripheral blood of CO_2-euthanized donor mice harboring 5−10% parasitemia by inoculation in the lateral vein of the tail.

Before drug administration, each infected mouse was randomly assigned to its corresponding treatment. Drug treatment started at ∼1.3% patent parasitemia (day 1). The treatment was administered by oral gavage with 20G straight reusable feeding needles (Fine Science Tools GmbH) at 10 mL/kg bodyweight unless otherwise stated.

Parasitemia was measured in serial 2 μL samples of tail blood by flow cytometry and expressed as the % of parasitized erythrocytes with respect to the total erythrocytes in circulation. A qualitative analysis of the effect of treatment on *P. falciparum* Pf3D70087/N9 was assessed by microscopy with Giemsa-stained blood smears and flow cytometry by staining with TER-119-Phycoerythrine (marker of murine erythrocytes) and SYTO-16 (nucleic acid dye) and acquisition in an Attune NxT Acoustic Focusing Flow Cytometer (InvitroGen), as previously described.[68] The levels of drugs were measured in samples of peripheral blood (25 μL) taken at different times after the first dosing, mixed with 25 μL of Milli-Q H_2O, and immediately frozen on a thermal block at −80 °C. The frozen samples were stored at −80 °C until analysis. Blood from control humanized mice was used for the preparation of standard curves, calibration, and quality control purposes. The drugs were extracted from 10 μL of lysates obtained by protein precipitation of blood samples using standard liquid−liquid extraction methods. The samples are analyzed by liquid chromatography with tandem mass spectrometry (LC-MS/MS) for quantification in a Waters Micromass UPLC-TQD (Waters, Manchester, U.K.). Blood concentration vs time was analyzed by noncompartmental analysis (NCA) using Phoenix WinNonlin vers.9.2 (Certara) or R or Excel (Microsoft), from which exposure-related values (T_{max}, C_{max}, and AUC_{0-t}) were estimated.

The rate of parasite clearance was assessed as the parasite reduction ratio (PRR) calculated as the ratio between parasitemia at day n + 2 divided by parasitemia at day n for each individual of the study. The day of recrudescence (DoR) was calculated for the mice that showed a decline of parasitemia below parasitemia at treatment inception (P0) and a subsequent growth up to P0. DoR was estimated by linear interpolation of % parasitemia the day before the rise to P0 and the % parasitemia the day after reaching P0 as described.[55] The mice were deemed cured if they were free of detectable parasite in peripheral blood by flow cytometry at a 0.01% limit of quantification by day 60 of the study.

4.9. In Vivo Prophylactic Liver Studies Using *P. berghei* in B6/Albino Mice. On the day of the experiment, naive C57BL/6 albino female mice were infected intravenously with 20,000 *P. berghei* sporozoites from the reporter line $PbmCherry_{hsp70}$ + $Luc_{eef1\alpha}$ that expresses mCherry reporter under the control of the hsp70 5′- and 3′-regulatory sequences and luciferase under the control of the ee1fα 5′-promoter/regulatory sequences.[69] Experimental mice were orally treated (p.o.) 24 and 48 h post-infection, using a volume of administration of 10 mL/kg at a compound concentration of 5 mg/mL. The parasite load was determined by bioluminescence in the liver 24 and 48 h post-infection, and in the peripheral blood 72 h post-infection and compared to the untreated control group. (The mice were anesthetized with isoflurane after an injection of Luciferin (80 mg/mL solution) with a volume of 1.5 mL/kg IV, and bioluminescence was recorded with a highly sensitive charge-coupled device (CCD) camera with a LuminaII in vivo imager.) A liver load reduction of less than 40% is usually considered a lack of activity in the liver stages. Blood stage infection was microscopically monitored regularly from 72 h post-infection via Giemsa-stained blood smears, up to >30 days post-infection, at which point a compound is considered curative in the absence of detectable blood stages.

The blood levels of the compound were evaluated to obtain standard pharmacokinetic parameters. Peripheral blood samples (20 μL) were collected 2, 24, 48, and 72 h post first administration, mixed with 20 μL of Milli-Q H_2O, immediately frozen on dry ice, and stored at −80 °C until analysis. Blood from control mice was used for calibration and QC purposes. Blood samples were processed under standard liquid−liquid extraction conditions and analyzed by LC-MS/MS for quantification by Swiss BioQuant (Basel, Switzerland).

■ ASSOCIATED CONTENT

Supporting Information

The Supporting Information is available free of charge at https://pubs.acs.org/doi/10.1021/acs.jmedchem.2c01336.

^{1}H NMR spectra of compounds **1**−**5** and **UCB7362** as well as intermediates **7**−**17**; ^{13}C NMR spectra of compounds **1**, **2**, **3**, **5**, and **UCB7362**; UPLC traces of compound **3** and **UCB7362**; absolute stereochemistry determination of intermediate **17** using vibrational circular dichroism; data collation of refinements of structure solution of *Pf*PMX bound to compound **4**; PMX activity of the isomers at the THP ring for compound **3**; whole-genome sequencing data for resistance parasites; complementary data for the pharmacokinetic model (Figure 5B,D); in vitro pharmacology methods and physicochemical and drug metabolism pharmacokinetics (DMPK) assays; and in vivo PK studies, human PK predictions, and in vitro and in vivo safety profiling (PDF)

Molecular formula strings for compounds **1**−**5** and **UCB7362** and biological data (CSV)

Accession Codes

The X-ray cocrystal structure of compound **4** bound to PMX has been deposited in the Protein Data Bank with the PDB code 8DSR. Compound ID in the PDB is TWU. The authors will release the atomic coordinates upon article publication.

https://doi.org/10.1021/acs.jmedchem.2c01336
J. Med. Chem. 2022, 65, 14121−14143

AUTHOR INFORMATION

Corresponding Authors

Benoît Laleu − *Medicines for Malaria Venture, 1215 Geneva, Switzerland;* orcid.org/0000-0002-7530-2113; Email: laleub@mmv.org

Teresa de Haro − *UCB, 1420 Braine-l'Alleud, Belgium;* orcid.org/0000-0002-6860-3970; Email: Teresa.DeHaroGarcia@ucb.com

Authors

Martin A. Lowe − *UCB, Slough SL1 3WE, United Kingdom;* Present Address: Exscientia, Oxford Science Park, The Schrödinger Building, Oxford OX4 4GE, United Kingdom

Alvaro Cardenas − *UCB, 1420 Braine-l'Alleud, Belgium*

Jean-Pierre Valentin − *UCB, 1420 Braine-l'Alleud, Belgium*

Zhaoning Zhu − *UCB, Slough SL1 3WE, United Kingdom;* Present Address: 12355 Fairway Pointe Row, San Diego, California 92128, United States.

Jan Abendroth − *UCB, Bainbridge Island, Washington 98110, United States*

Jose L. Castro − *UCB, Slough SL1 3WE, United Kingdom*

Reiner Class − *UCB, 1420 Braine-l'Alleud, Belgium*

Annie Delaunois − *UCB, 1420 Braine-l'Alleud, Belgium;* orcid.org/0000-0001-6345-7989

Renaud Fleurance − *UCB, 1420 Braine-l'Alleud, Belgium*

Helga Gerets − *UCB, 1420 Braine-l'Alleud, Belgium;* orcid.org/0000-0003-3199-950X

Vitalina Gryshkova − *UCB, 1420 Braine-l'Alleud, Belgium*

Lloyd King − *UCB, Slough SL1 3WE, United Kingdom*

Donald D. Lorimer − *UCB, Bainbridge Island, Washington 98110, United States*

Malcolm MacCoss − *Bohicket Pharma Consulting LLC, Seabrook Island, South Carolina 29455, United States*

Julian H. Rowley − *UCB, Slough SL1 3WE, United Kingdom;* orcid.org/0000-0002-9419-6483

Marie-Luce Rosseels − *UCB, 1420 Braine-l'Alleud, Belgium*

Leandro Royer − *UCB, 1420 Braine-l'Alleud, Belgium*

Richard D. Taylor − *UCB, Slough SL1 3WE, United Kingdom;* orcid.org/0000-0002-4808-5010

Melanie Wong − *UCB, Slough SL1 3WE, United Kingdom*

Oliver Zaccheo − *UCB, Slough SL1 3WE, United Kingdom*

Vishal P. Chavan − *Sai Life Sciences Limited, Hyderabad 500078 Telangana, India*

Gokul A. Ghule − *Sai Life Sciences Limited, Hyderabad 500078 Telangana, India*

Bapusaheb K. Tapkir − *Sai Life Sciences Limited, Hyderabad 500078 Telangana, India*

Jeremy N. Burrows − *Medicines for Malaria Venture, 1215 Geneva, Switzerland;* orcid.org/0000-0001-8448-6068

Maëlle Duffey − *Medicines for Malaria Venture, 1215 Geneva, Switzerland*

Matthias Rottmann − *Swiss Tropical and Public Health Institute, CH-4123 Allschwil, Switzerland; University of Basel, 4002 Basel, Switzerland*

Sergio Wittlin − *Swiss Tropical and Public Health Institute, CH-4123 Allschwil, Switzerland; University of Basel, 4002 Basel, Switzerland*

Iñigo Angulo-Barturen − *The Art of Discovery, 48160 Bizkaia, Basque Country, Spain*

María Belén Jiménez-Díaz − *The Art of Discovery, 48160 Bizkaia, Basque Country, Spain*

Josefine Striepen − *Department of Microbiology & Immunology, Columbia University Irving Medical Center, New York, New York 10032, United States*

Kate J. Fairhurst − *Department of Microbiology & Immunology, Columbia University Irving Medical Center, New York, New York 10032, United States*

Tomas Yeo − *Department of Microbiology & Immunology, Columbia University Irving Medical Center, New York, New York 10032, United States*

David A. Fidock − *Department of Microbiology & Immunology, Columbia University Irving Medical Center, New York, New York 10032, United States; Center for Malaria Therapeutics and Antimicrobial Resistance, Division of Infectious Diseases, Department of Medicine, Columbia University Irving Medical Center, New York, New York 10032, United States*

Alan F. Cowman − *The Walter and Eliza Hall Institute of Medical Research, Parkville, VIC 3052, Australia*

Paola Favuzza − *The Walter and Eliza Hall Institute of Medical Research, Parkville, VIC 3052, Australia*

Benigno Crespo-Fernandez − *Global Health, GlaxoSmithKline R&D, 28760 Madrid, Spain*

Francisco Javier Gamo − *Global Health, GlaxoSmithKline R&D, 28760 Madrid, Spain;* orcid.org/0000-0002-1854-2882

Daniel E. Goldberg − *Division of Infectious Diseases, Department of Medicine, Washington University School of Medicine, St. Louis, Missouri 63110, United States;* orcid.org/0000-0003-3529-8399

Dominique Soldati-Favre − *Department of Microbiology and Molecular Medicine, Faculty of Medicine, CMU, CH-1211 Genève 4, Switzerland*

Complete contact information is available at: https://pubs.acs.org/10.1021/acs.jmedchem.2c01336

Author Contributions

The manuscript was written through contributions of all authors. All authors have given approval to the final version of the manuscript.

Funding

This work was funded by UCB with generous support from Medicines for Malaria Venture (MMV) (RD-15-0043) and through their assay support network.

Notes

The authors declare no competing financial interest.

The authors declare the following financial interest(s): M.A.L., A.C., J.-P.V., Z.Z., J.A., J.L.C., R.C., A.D., R.F., H.G., V.G., L.K., D.D.L., J.H.R., M.-L.R., L.R., R.D.T., M.W., O.Z., and T.d.H. are UCB employees; J.N.B., M.D., and B.L. are MMV employees; B.C.-F. and F.J.G. are GSK employees.

ACKNOWLEDGMENTS

The authors acknowledge the synthetic contributions of our colleagues at Sai Life Sciences, especially Vivek Humne for the synthesis of compound 2, WuXi AppTech, and TCGLS, especially Abhijit Kundu, Subrata Chattopadhyay, and Rajib Barik. They thank the Drug Discovery Unit from the University of Dundee for having generated 3D7 data (SYBR green as readout) in the early stages of the project, especially Mark Anderson and Irene Hallyburton. They also thank Sibylle Sax and Christian Scheurer (STPH) for their support in the in vitro assays related to the panel of *Pf* strains. Thanks also go to

Christoph Fischli for his support with the in vivo prophylactic *P. berghei* liver model. The authors also thank the study director and contract research organizations (CROs) where each of the safety studies has been performed: Genotox MN: Robert Smith from Lapcorp. Genotox ames: Rizwan Nisar and Lucinda Lill-ford from Lapcorp. Phototox MEC: Magdalena Kierkowicz from UCB. Phototox 3T3: Jet Gijsbrecht from Charles River DenBosch. Biotrial, B'SYS GmbH, Eurofins Discovery, and Physiostim. In vivo 7D tox study: Bailey Melanie and Joffrey Ducroq from Charles River Lyon. The authors also thank all associates at MMV, especially Fanny Escudié, Benjamin Blasco, and Elodie Chenu, as well as MMV partners and their Network, especially Belen Tornesi and Jane Stewart. The authors are grateful to UCB team members that have contributed to the project over the years. Specially to Nabila Chabbi as the nonclinical formulation lead and Mark Penney for PKPD discussions.

■ ABBREVIATIONS USED

ADME, absorption−distribution−metabolism−excretion; AUC, area under the curve; bid, bis in die; Cbz, benzyloxy carbamate; CCD, charge-coupled device; CL, clearance; CNV, copy number variation; CRO, contract research organization; CYP450, cytochrome P450; DCM, dichloromethane; DDI, drug−drug interaction; DHA, dihydroartemisinin; DIPEA, *N*,*N*-diisopropylethylamine; DMPK, drug metabolism pharmacokinetics; DMF, dimethyl formamide; DMSO, dimethylsulfoxide; EDCI, 1-ethyl-3-(3-dimethylaminopropyl)carbodiimide; EDC·HCl, *N*-(3-dimethylaminopropyl)-*N*′-ethylcarbodiimide hydrochloride; EC_{50}, half-maximal effective concentration; EC_{90}, 90% effective concentration; EC_{20}, 20% effective concentration; ESI, electrospray ionization; EtOAc, ethyl acetate; Fu, fraction unbound; F, bioavailability; FRET, fluorescence resonance energy transfer; GlcN, glucosamine; HCl, hydrochloride; hERG, human ether-a-go-go related gene; HEPES, 4-(2-hydroxyethyl)-1-piperazineethanesulfonic acid; HPLC, high-performance liquid chromatography; HRMS, high-resolution mass spectroscopy; IC_{50}, half-maximal inhibitory concentration; IC_{90}, 90% inhibitory concentration; IP, intraperitoneal; IV, intravenous; LBF, liver blood flow; LDH, lactate dehydrogenase; LCMS, liquid chromatography−mass spectrometry; MeOH, methanol; MES, 2-(*N*-morpholino)-ethanesulfonic acid; MS, mass spectroscopy; MOPS, 3-(*N*-morpholino)propanesulfonic acid; MW, molecular weight; NMR, nuclear magnetic resonance; NOD-SCID, nonobese diabetic severe combined immunodeficient; PE, petroleum ether; PO, per oral; RT, room temperature; SAR, structure−activity relationship; SDS PAGE, sodium dodecyl sulfate-polyacrylamide gel electrophoresis; SNPs, single-nucleotide polymorphisms; THF, tetrahydrofuran; TFA, trifluoroacetic acid; TFAA, trifluoroacetic anhydride; TEA, triethylamine; TBME, *tert*-butyl methyl ether; TCEP, tris(2-carboxyethyl)-phosphine; TLC, thin-layer chromatography; TEV, tobacco etch virus; TOF MS, time-of-flight mass spectrometry; UPLC, ultraperformance liquid chromatography; VCD, vibrational circular dichroism

■ REFERENCES

(1) WHO. *World Malaria Report 2021*; World Health Organization: Geneva, 2021.
(2) Burrows, J. N.; Duparc, S.; Gutteridge, W. E.; van Huijsduijnen, R. H.; Kaszubska, W.; Macintyre, F.; Mazzuri, S.; Möhrle, J. J.; Wells, T. N. C. New developments in antimalarial target candidate and product profiles. *Malar. J.* **2017**, *16*, No. 26.
(3) Cai, H.; Kuang, R.; Gu, J.; Wang, Y. Proteases in malaria parasites - a phylogenomic perspective. *Curr. Genomics* **2011**, *12*, 417−427.
(4) Cheuka, P. M.; Dziwornu, G.; Okombo, J.; Chibale, K. Plasmepsin inhibitors in antimalarial drug discovery: Medicinal chemistry and target validation (2000 to Present). *J. Med. Chem.* **2020**, *63*, 4445−4467.
(5) Mishra, M.; Singh, V.; Singh, S. Structural Insights into key Plasmodium proteases as therapeutic drug targets. *Front. Microbiol.* **2019**, *10*, No. 394.
(6) Nasamu, A. S.; Polino, A. J.; Istvan, E. S.; Goldberg, D. E. Malaria parasite plasmepsins: More than just plain old degradative pepsins. *J. Biol. Chem.* **2020**, *295*, 8425−8441.
(7) Beck, J. R.; Ho, C. M. Transport mechanisms at the malaria parasite-host cell interface. *PLoS Pathog.* **2021**, *17*, No. e10093946061.
(8) Dogga, S. K.; Mukherjee, B.; Jacot, D.; Kockmann, T.; Molino, L.; Hammoudi, P.-M.; Hartkoorn, R. C.; Hehl, A. B.; Soldati-Favre, D. A druggable secretory protein maturase of Toxoplasma essential for invasion and egress. *eLife* **2017**, *6*, No. e27480.
(9) Cowman, A. F.; Berry, D.; Baum, J. The cellular and molecular basis for malaria parasite invasion of the human red blood cell. *J. Cell Biol.* **2012**, *198*, 961−971.
(10) Munsamy, G.; Ramharacka, P.; Soliman, M. E. S. Egress and invasion machinery of malaria: an in-depth look into the structural and functional features of the flap dynamics of plasmepsin IX and X. *RSC Adv.* **2018**, *8*, 21829−21840.
(11) Pino, P.; Caldelari, R.; Mukherjee, B.; Vahokoski, J.; Klages, N.; Maco, B.; Collins, C. R.; Blackman, M. J.; Kursula, I.; Heussler, V.; Brochet, M.; Soldati-Favre, D. A. Multistage antimalarial targets the plasmepsins IX and X essential for invasion and egress. *Science* **2017**, *358*, 522−528.
(12) Nasamu, A. S.; Glushakova, S.; Russo, I.; Vaupel, B.; Oksman, A.; Kim, A. S.; Fremont, D. H.; Tolia, N.; Beck, J. R.; Meyers, M. J.; Niles, J. C.; Zimmerberg, J.; Goldberg, D. E. Plasmepsins IX and X are essential and druggable mediators of malaria parasite egress and invasion. *Science* **2017**, *358*, 518−522.
(13) Favuzza, P.; de Lera Ruiz, M.; Thompson, J. K.; Triglia, T.; Ngo, A.; Steel, R. W. J.; Vavrek, M.; Christensen, J.; Healer, J.; Boyce, C.; Guo, Z.; Hu, M.; Khan, T.; Murgolo, N.; Zhao, L.; Penington, J. S.; Reaksudsan, K.; Jarman, K.; Dietrich, M. H.; Richardson, L.; Guo, K. Y.; Lopaticki, S.; Tham, W. H.; Rottmann, M.; Papenfuss, T.; Robbins, J. A.; Boddey, J. A.; Sleebs, B. E.; Sabroux, H. J.; McCauley, J. A.; Olsen, D. B.; Cowman, A. F. Dual plasmepsin-targeting antimalarial agents disrupt multiple stages of the malaria parasite life cycle. *Cell Host Microbe* **2020**, *27*, 642−658.
(14) Munsamy, G.; Agoni, C.; Soliman, M. E. S. A dual target of Plasmepsin IX and X: Unveiling the atomistic superiority of a core chemical scaffold in malaria therapy. *J. Cell. Biochem.* **2019**, *120*, 7876−7887.
(15) Mukherjee, B.; Tessaro, F.; Vahokoski, J.; Kursula, I.; Marq, J. B.; Scapozza, L.; Soldati-Favre, D. Modeling and resistant alleles explain the selectivity of antimalarial compound 49c towards apicomplexan aspartyl proteases. *EMBO J.* **2018**, *37*, No. e98047.
(16) Hodder, A. N.; Christensen, J.; Scally, S.; Triglia, T.; Ngo, A.; Birkinshaw, R. W.; Bailey, B.; Favuzza, P.; Dietrich, M. H.; Tham, W. H.; Czabotar, P. E.; Lowes, K.; Guo, Z.; Murgolo, N.; Lera Ruiz, M.; McCauley, J. A.; Sleebs, B. E.; Olsen, D.; Cowman, A. F. Basis for drug selectivity of plasmepsin IX and X inhibition in *Plasmodium falciparum* and *vivax*. *Structure* **2022**, *30*, 947.e6.
(17) Kesari, P.; Deshmukh, A.; Pahelkar, N.; Suryawanshi, A. B.; Rathore, I.; Mishra, V.; Dupuis, J. H.; Xiao, H.; Gustchina, A.; Abendroth, J.; Labaied, M.; Yada, R. Y.; Wlodawer, A.; Edwards, T. E.; Lorimer, D. D.; Bhaumik, P. Structures of plasmepsin X from *Plasmodium falciparum* reveal a novel inactivation mechanism of the zymogen and molecular basis for binding of inhibitors in mature enzyme. *Protein Sci.* **2022**, *31*, 882−899.

https://doi.org/10.1021/acs.jmedchem.2c01336
J. Med. Chem. 2022, 65, 14121−14143

(18) Zhu, Z. Iminoheterocycle as a druggable motif: BACE1 inhibitors and beyond. *Trends Pharmacol. Sci.* **2012**, *33*, 233−240.
(19) Gamo, F. J.; Sanz, L. M.; Vidal, J.; de Cozar, C.; Alvarez, E.; Lavandera, J. L.; Vanderwall, D. E.; Green, D. V.; Kumar, V.; Hasan, S.; Brown, J. R.; Peishoff, C. E.; Cardon, L. R.; Garcia-Bustos, J. F. Thousands of chemical starting points for antimalarial lead identification. *Nature* **2010**, *465*, 305−310.
(20) Calderón, F.; Barros, D.; Bueno, J. M.; Coteròn, J. M.; Fernà ndez, E.; Gamo, F. J.; Lavandera, J. L.; Leon, M. L.; Macdonald, S. J. F.; Mallo, A.; Manzano, P.; Porras, E.; Fiandor, J. M.; Castro, J. An invitation to open innovation in malaria drug discovery: 47 quality starting points from the TCAMS. *ACS Med. Chem. Lett.* **2011**, *2*, 741−746.
(21) Meyers, M. J.; Tortorella, M. D.; Xu, J.; Qin, L.; He, Z.; Lang, X.; Zeng, W.; Xu, W.; Qin, L.; Prinsen, M. J.; Sverdrup, F. M.; et al. Evaluation of aminohydantoins as a novel class of antimalarial agents. *ACS Med. Chem. Lett.* **2014**, *5*, 89−93.
(22) Zhu, Z.; Sun, Z. Y.; Ye, Y.; Voigt, J.; Strickland, C.; Smith, E. M.; Cumming, J.; Wang, L.; Wong, J.; Wang, Y. S.; Wyss, D. F.; Chen, X.; Kuvelkar, R.; Kennedy, M. E.; Favreau, L.; Parker, E.; McKittrick, B. A.; Stamford, A.; Czarniecki, M.; Greenlee, W.; Hunter, J. C. Discovery of cyclic acylguanidines as highly potent and selective beta-site amyloid cleaving enzyme (BACE) inhibitors: Part I–inhibitor design and validation. *J. Med. Chem.* **2010**, *53*, 951−965.
(23) Coimbra, J. R. M.; Marques, D. F. F.; Baptista, S. J.; Pereira, C. M. F.; Moreira, P. I.; Dinis, T. C. P.; Santos, A. E.; Salvador, J. A. R. Highlights in BACE1 inhibitors for alzheimer's disease treatment. *Front. Chem.* **2018**, *6*, No. 178.
(24) Ghosh, A. K.; Osswald, H. L. BACE1 (β-secretase) inhibitors for the treatment of Alzheimer's disease. *Chem. Soc. Rev.* **2014**, *43*, 6765−6813.
(25) Kennedy, M. E.; Stamford, A. W.; Chen, X.; Cox, K.; Cumming, J. N.; Dockendorf, M. F.; Egan, M.; Ereshefsky, L.; Hodgson, R. A.; Hyde, L. A.; Jhee, S.; Kleijn, H. J.; Kuvelkar, R.; Li, W.; Mattson, B. A.; Mei, H.; Palcza, J.; Scott, J. D.; Tanen, M.; Troyer, M. D.; Tseng, J. L.; Stone, J. A.; Parker, E. M.; Forman, M. S. The BACE1 inhibitor verubecestat (MK-8931) reduces CNS β-amyloid in animal models and in Alzheimer's disease patients. *Sci. Transl. Med.* **2016**, *8*, No. 363ra150.
(26) Yadati, T.; Houben, T.; Bitorina, A.; Shiri-Sverdlov, R. The ins and outs of cathepsins: physiological function and role in disease management. *Cells* **2020**, *9*, No. 1679.
(27) Barber, J.; Sikakana, P.; Sadler, C.; Baud, D.; Valentin, J. P.; Roberts, R. A target safety assessment of the potential toxicological risks of targeting plasmepsin IX/X for the treatment of malaria. *Toxicol. Res.* **2021**, *10*, 203−213.
(28) Xu, Y.; Li, M. J.; Greenblatt, H.; Chen, W.; Paz, A.; Dym, O.; Peleg, Y.; Chen, T.; Shen, X.; He, J.; Jiang, H.; Silman, I.; Sussman, J. L. Flexibility of the flap in the active site of BACE1 as revealed by crystal structures and molecular dynamics simulations. *Acta Crystallogr., Sect. D: Biol. Crystallogr.* **2012**, *68*, 13−25.
(29) Bowes, J.; Brown, A.; Hamon, J.; Jarolimek, W.; Sridhar, A.; Waldron, G.; Whitebread, S. Reducing safety-related drug attrition: the use of in vitro pharmacological profiling. *Nat. Rev. Drug Discovery* **2012**, *11*, 909−922.
(30) Chambers, R. K.; Khan, T. A.; Olsen, D. B.; Sleebs, B. E. Synthesis of amino heterocycle aspartyl protease inhibitors. *Org. Biomol. Chem.* **2016**, *14*, 4970−4985.
(31) Ding, X. C.; Ubben, D.; Wells, T. N. A framework for assessing the risk of resistance for anti-malarials in development. *Malar. J.* **2012**, *11*, No. 292.
(32) Snyder, C.; Chollet, J.; Santo-Tomas, J.; Scheurer, C.; Wittlin, S. In vitro and in vivo interaction of synthetic peroxide RBx11160 (OZ277) with piperaquine in *Plasmodium* models. *Exp. Parasitol.* **2007**, *115*, 296−300.
(33) Ashton, T. D.; Devine, S. M.; Möhrle, J. J.; Laleu, B.; Burrows, J. N.; Charman, S. A.; Creek, D. J.; Sleebs, B. E. Development of the most clinically advanced modern antimalarials. *J. Med. Chem.* **2019**, *62*, 10526−10562.
(34) Ross, L. S.; Dhingra, S. K.; Mok, S.; Yeo, T.; Wicht, K. J.; Kümpornsin, K.; Takala-Harrison, S.; Witkowski, B.; Fairhurst, R. M.; Ariey, F.; Menard, D.; Fidock, D. A. Emerging Southeast Asian PfCRT mutations confer *Plasmodium falciparum* resistance to the first-line antimalarial piperaquine. *Nat. Commun.* **2018**, *9*, No. 3314.
(35) Paquet, T.; Le Manach, C.; Cabrera, D. G.; Younis, Y.; Henrich, P. P.; Abraham, T. S.; Lee, M. C. S.; Basak, R.; Ghidelli-Disse, S.; Lafuente-Monasterio, M. J.; Bantscheff, M.; Ruecker, A.; Blagborough, A. M.; Zakutansky, S. E.; Zeeman, A. M.; White, K. L.; Shackleford, D. M.; Mannila, J.; Morizzi, J.; Scheurer, C.; Angulo-Barturen, I.; Martinez, M. S.; Ferrer, S.; Sanz, L. M.; Gamo, F. J.; Reader, J.; Botha, M.; Dechering, K. J.; Sauerwein, R. W.; Tungtaeng, A.; Vanachayangkul, P.; Lim, C. S.; Burrows, J.; Witty, M. J.; Marsh, K. C.; Bodenreider, C.; Rochford, R.; Solapure, S. M.; Jimenez-Diaz, M. B.; Wittlin, S.; Charman, S. A.; Donini, C.; Campo, B.; Birkholtz, L. M.; Hanson, K. K.; Drewes, G.; Kocken, C. H. M.; Delves, M. J.; Leroy, D.; Fidock, D. A.; Waterson, D.; Street, L. J.; Chibale, K. Antimalarial efficacy of MMV390048, an inhibitor of Plasmodium phosphatidylinositol 4-kinase. *Sci. Transl. Med.* **2017**, *9*, No. eaad9735.
(36) Baragaña, B.; Hallyburton, I.; Lee, M. C.; Norcross, N. R.; Grimaldi, R.; Otto, T. D.; Proto, W. R.; Blagborough, A. M.; Meister, S.; Wirjanata, G.; Ruecker, A.; Upton, L. M.; Abraham, T. S.; Almeida, M. J.; Pradhan, A.; Porzelle, A.; Martínez, M. S.; Bolscher, J. M.; Woodland, A.; Luksch, T.; Norval, S.; Zuccotto, F.; Thomas, J.; Simeons, F.; Stojanovski, L.; Osuna-Cabello, M.; Brock, P. M.; Churcher, T. S.; Sala, K. A.; Zakutansky, S. E.; Jiménez-Díaz, M. B.; Sanz, L. M.; Riley, J.; Basak, R.; Campbell, M.; Avery, V. M.; Sauerwein, R. W.; Dechering, K. J.; Noviyanti, R.; Campo, B.; Frearson, J. A.; Angulo-Barturen, I.; Ferrer-Bazaga, S.; Gamo, F. J.; Wyatt, P. G.; Leroy, D.; Siegl, P.; Delves, M. J.; Kyle, D. E.; Wittlin, S.; Marfurt, J.; Price, R. N.; Sinden, R. E.; Winzeler, E. A.; Charman, S. A.; Bebrevska, L.; Gray, D. W.; Campbell, S.; Fairlamb, A. H.; Willis, P. A.; Rayner, J. C.; Fidock, D. A.; Read, K. D.; Gilbert, I. H. A novel multiple-stage antimalarial agent that inhibits protein synthesis. *Nature* **2015**, *522*, 315−320.
(37) Phillips, M. A.; Lotharius, J.; Marsh, K.; White, J.; Dayan, A.; White, K. L.; Njoroge, J. W.; El Mazouni, F.; Lao, Y.; Kokkonda, S.; Tomchick, D. R.; Deng, X.; Laird, T.; Bhatia, S. N.; March, S.; Ng, C. L.; Fidock, D. A.; Wittlin, S.; Lafuente-Monasterio, M.; Benito, F. J.; Alonso, L. M.; Martinez, M. S.; Jimenez-Diaz, M. B.; Bazaga, S. F.; Angulo-Barturen, I.; Haselden, J. N.; Louttit, J.; Cui, Y.; Sridhar, A.; Zeeman, A. M.; Kocken, C.; Sauerwein, R.; Dechering, K.; Avery, V. M.; Duffy, S.; Delves, M.; Sinden, R.; Ruecker, A.; Wickham, K. S.; Rochford, R.; Gahagen, J.; Iyer, L.; Riccio, E.; Mirsalis, J.; Bathhurst, I.; Rueckle, T.; Ding, X.; Campo, B.; Leroy, D.; Rogers, M. J.; Rathod, P. K.; Burrows, J. N.; Charman, S. A. A long-duration dihydroorotate dehydrogenase inhibitor (DSM265) for prevention and treatment of malaria. *Sci. Transl. Med.* **2015**, *7*, No. 296ra111.
(38) Stickles, A. M.; de Almeida, M. J.; Morrisey, J. M.; Sheridan, K. A.; Forquer, I. P.; Nilsen, A.; Winter, R. W.; Burrows, J. N.; Fidock, D. A.; Vaidya, A. B.; Riscoe, M. K. Subtle changes in endochin-like quinolone structure alter the site of inhibition within the cytochrome bc1 complex of *Plasmodium falciparum*. *Antimicrob. Agents Chemother.* **2015**, *59*, 1977−1982.
(39) Meister, S.; Plouffe, D. M.; Kuhen, K. L.; Bonamy, G. M. C.; Wu, T.; Barnes, S. W.; Bopp, S. E.; Borboa, R.; Bright, A. T.; Jianwei Che, J.; Cohen, S.; Dharia, N. V.; Gagaring, K.; Gettayacamin, M.; Gordon, P.; Groessl, T.; Kato, N.; Lee, M. C. S.; McNamara, C. W.; Fidock, D. A.; Nagle, A.; Nam, T.-G.; Richmond, W.; Roland, J.; Rottmann, M.; Zhou, B.; Froissard, P.; Glynne, R. J.; Mazier, D.; Sattabongkot, J.; Schultz, P. G.; Tuntland, T.; Walker, J. R.; Zhou, Y.; Chatterjee, A.; Diagana, T. T.; Winzeler, E. A. Imaging of Plasmodium liver stages to drive next-generation antimalarial drug discovery. *Science* **2011**, *334*, 1372−1377.
(40) When PMX is HA-tagged it seems to have an effect on IC_{50} with some compounds—not all. This may be because the HA-tag is affecting access or binding to the active site for particular compounds. For **UCB7362** once PMX is HA-tagged it becomes considerably more sensitive.

https://doi.org/10.1021/acs.jmedchem.2c01336
J. Med. Chem. 2022, 65, 14121−14143

(41) Dziekan, J. M.; Wirjanata, G.; Dai, L.; Go, K.; Yu, H.; Lim, Y.-T.; Chen, L.; Wang, L.; Puspita, B.; Prabhu, N.; Sobota, R.; Nordlund, P.; Bozdech, Z. Cellular thermal shift assay for the identification of drug−target interactions in the *Plasmodium falciparum* proteome. *Nat. Protoc.* **2020**, *15*, 1881−1921.
(42) Dziekan, J. M.; Yu, H.; Chen, D.; Dai, L.; Wirjanata, G.; Larsson, A.; Prabhu, N.; Sobota, R. M.; Bozdech, Z.; Nordlund, P. Identifying purine nucleoside phosphorylase as the target of quinine using cellular thermal shift assay. *Sci. Transl. Med.* **2019**, *11*, No. eaau3174.
(43) Duffey, M.; Blasco, B.; Burrows, J. N.; Wells, T. N. C.; Fidock, D. A.; Leroy, D. Assessing risks of *Plasmodium falciparum* resistance to select next-generation antimalarials. *Trends Parasitol.* **2021**, *37*, 709−721.
(44) Wicht, K. J.; Mok, S.; Fidock, D. A. Molecular Mechanisms of Drug Resistance in *Plasmodium falciparum* Malaria. *Annu. Rev. Microbiol.* **2020**, *74*, 431−454.
(45) Blasco, B.; Leroy, D.; Fidock, D. A. Antimalarial drug resistance: linking *Plasmodium falciparum* parasite biology to the clinic. *Nat. Med.* **2017**, *23*, 917−928.
(46) Koussis, K.; Withers-Martinez, C.; Yeoh, S.; Child, M.; Hackett, F.; Knuepfer, E.; Juliano, L.; Woehlbier, U.; Bujard, H.; Blackman, M. J. A multifunctional serine protease primes the malaria parasite for red blood cell invasion. *EMBO J.* **2009**, *28*, 725−35.
(47) Sanz, L. M.; Crespo, B.; De-Cózar, C.; Ding, X. C.; Llergo, J. L.; Burrows, J. N.; García-Bustos, J. F.; Gamo, F. J. *P. falciparum* in vitro killing rates allow to discriminate between different antimalarial mode-of-action. *PLoS One* **2012**, *7*, No. e30949.
(48) Jiménez-Díaz, M. B.; Mulet, T.; Viera, S.; Gómez, V.; Garuti, H.; Ibáñez, J.; Alvarez-Doval, A.; Shultz, L. D.; Martínez, A.; Gargallo-Viola, D.; Angulo-Barturen, I. Improved murine model of malaria using *Plasmodium falciparum* competent strains and nonmyelodepleted NOD-scid IL2Rγnull mice engrafted with human erythrocytes. *Antimicrob. Agents Chemother.* **2009**, *53*, 4533−4536.
(49) Demarta-Gatsi, C.; Andenmatten, N.; Jiménez-Díaz, M. B.; Gobeau, N.; Cherkaoui, M.; Fuchs, A.; Díaz, P.; Berja, S.; Sánchez, R.; Gómez, H.; Ruiz, E.; Sainz, P.; Salazar, E.; Gil-Merino, R.; Mendoza, L. M.; Eguizabal, C.; Leroy, D.; Möhrle, J. J.; Tornesi, B.; Angulo-Barturen, I. Predicting Optimal Antimalarial Drug Combinations from a Standardized *P. falciparum* Humanized Mouse Model. Unpublished Results.
(50) See Supporting Information for more details.
(51) Yamagata, T.; Zanelli, U.; Gallemann, D.; Perrin, D.; Dolgos, H.; Petersson, C. Comparison of methods for the prediction of human clearance from hepatocyte intrinsic clearance for a set of reference compounds and an external evaluation set. *Xenobiotica* **2017**, *47*, 741−751.
(52) Berezhkovskiy, L. M. The corrected traditional equations for calculation of hepatic clearance that account for the difference in drug ionization in extracellular and intracellular tissue water and the corresponding corrected PBPK equation. *J. Pharm. Sci.* **2011**, *100*, 1167−1183.
(53) Berry, L. M.; Li, C.; Zhao, Z. Species differences in distribution and prediction of human Vss from preclinical data. *Drug Metab. Dispos.* **2011**, *39*, 2103−2116.
(54) Sugano, K.; Terada, K. Rate- and extent-limiting factors of oral drug absorption: theory and applications. *J. Pharm. Sci.* **2015**, *104*, 2777−2788.
(55) Fielden, M. R.; Werner, J.; Jamison, J. A.; Coppi, A.; Hickman, D.; Dunn, R. T., 2nd; Trueblood, E.; Zhou, L.; Afshari, C. A.; Lightfoot-Dunn, R. Retinal toxicity induced by a novel β-secretase inhibitor in the Sprague-dawley rat. *Toxicol. Pathol.* **2015**, *43*, 581−592.
(56) Cai, J.; Qi, X.; Kociok, N.; Skosyrski, S.; Emilio, A.; Ruan, Q.; Han, S.; Liu, L.; Chen, Z.; Bowes Rickman, C.; Golde, T.; Grant, M. B.; Saftig, P.; Serneels, L.; de Strooper, B.; Joussen, A. M.; Boulton, M. E. β-Secretase (BACE1) inhibition causes retinal pathology by vascular dysregulation and accumulation of age pigment. *EMBO Mol. Med.* **2012**, *4*, 980−991.
(57) Zuhl, A. M.; Nolan, C. E.; Brodney, M. A.; Niessen, S.; Atchison, K.; Houle, C.; Karanian, D. A.; Ambroise, C.; Brulet, J. W.; Beck, E. M.; Doran, S. D.; O'Neill, B. T.; Am Ende, C. W.; Chang, C.; Geoghegan, K. F.; West, G. M.; Judkins, J. C.; Hou, X.; Riddell, D. R.; Johnson, D. S. Chemoproteomic profiling reveals that cathepsin D off-target activity drives ocular toxicity of β-secretase inhibitors. *Nat Commun.* **2016**, *7*, No. 13042.
(58) Nociari, M. M.; Kiss, S.; Rodriguez-Boulan, E. Lipofuscin Accumulation Into And Clearance From Retinal Pigment Epithelium Lysosomes: Physiopathology and Emerging Therapeutics. In *Lysosomes—Associated Diseases and Methods to Study Their Function*; Sharma, P. D., Ed.; IntechOpen: London, 2017.
(59) Zuhl, A. M.; Nolan, C. E.; Brodney, M. A.; Niessen, S.; Atchison, K.; Houle, C.; Karanian, D. A.; Ambroise, C.; Brulet, J. W.; Beck, E. M.; Doran, S. D.; O'Neill, B. T.; am Ende, C. W.; Chang, C.; Geoghegan, K. F.; West, G. M.; Judkins, J. C.; Hou, X.; Riddell, D. R.; Johnson, D. S. Chemoproteomic profiling reveals that cathepsin D off-target activity drives ocular toxicity of β-secretase inhibitors. *Nat. Commun.* **2016**, *7*, No. 13042.
(60) Read, R. J. Pushing the boundaries of molecular replacement with maximum likelihood. *Acta Crystallogr., Sect. D: Biol. Crystallogr.* **2001**, *57*, 1373−1382. Erratum in: Acta Crystallogr., Sect. D: Biol. Crystallogr. 2003, 59, 404.
(61) Emsley, P.; Lohkamp, B.; Scott, W. G.; Cowtan, K. Features and development of Coot. *Acta Crystallogr., Sect. D: Biol. Crystallogr.* **2010**, *66*, 486−501.
(62) Adams, P. D.; Grosse-Kunstleve, R. W.; Hung, L. W.; Ioerger, T. R.; McCoy, A. J.; Moriarty, N. W.; Read, R. J.; Sacchettini, J. C.; Sauter, N. K.; Terwilliger, T. C. PHENIX: building new software for automated crystallographic structure determination. *Acta Crystallogr., Sect. D: Biol. Crystallogr.* **2002**, *58*, 1948−1954.
(63) Davis, I. W.; Leaver-Fay, A.; Chen, V. B.; Block, J. N.; Kapral, G. J.; Wang, X.; Murray, L. W.; Arendall, W. B.; Snoeyink, J.; Richardson, J. S.; Richardson, D. C. MolProbity: all-atom contacts and structure validation for proteins and nucleic acids. *Nucleic Acids Res.* **2007**, *35*, W375−W383.
(64) Stokes, B. H.; Dhingra, S. K.; Rubiano; Mok, S.; Straimer, J.; Gnädig, N. F.; Deni, I.; Schindler, K. A.; Bath, J. R.; Ward, K. E.; Striepen, J.; Yeo, T.; Ross, L. S.; Legrand, E.; Ariey, F.; Cunningham, C. H.; Souleymane, I. M.; Gansané, A.; Nzoumbou-Boko, R.; Ndayikunda, C.; Kabanywanyi, A. M.; Uwimana, A.; Smith, S. J.; Kolley, O.; Ndounga, M.; Warsame, M.; Leang, R.; Nosten, F.; Anderson, T. J.; Rosenthal, P. J.; Ménard, D.; Fidock, D. A. *Plasmodium falciparum* K13 mutations in Africa and Asia impact artemisinin resistance and parasite fitness. *Elife* **2021**, *10*, No. e66277.
(65) Vanaerschot, M.; Murithi, J. M.; Pasaje, C. F. A.; Ghidelli-Disse, S.; Dwomoh, L.; Bird, M.; Spottiswoode, N.; Mittal, N.; Arendse, L. B.; Owen, E. S.; Wicht, K. J.; Siciliano, G.; Bösche, M.; Yeo, T.; Kumar, T. R. S.; Mok, S.; Carpenter, E. F.; Giddins, M. J.; Sanz, O.; Ottilie, S.; Alano, P.; Chibale, K.; Llinás, M.; Uhlemann, A. C.; Delves, M.; Tobin, A. B.; Doerig, C.; Winzeler, E. A.; Lee, M. C. S.; Niles, J. C.; Fidock, D. A. Inhibition of resistance-refractory *P. falciparum* kinase PKG delivers prophylactic, blood stage, and transmission-blocking antiplasmodial activity. *Cell Chem. Biol.* **2020**, *27*, 806−816.
(66) Jiménez-Díaz, M. B.; Mulet, T.; Viera, S.; Gómez, V.; Garuti, H.; Ibáñez, J.; Alvarez-Doval, A.; Shultz, L. D.; Martínez, A.; Gargallo-Viola, D.; Angulo-Barturen, I. Improved murine model of malaria using *Plasmodium falciparum* competent strains and non-myelodepleted NOD-scid IL2Rgammanull mice engrafted with human erythrocytes. *Antimicrob Agents Chemother.* **2009**, *53*, 4533−4536.
(67) Angulo-Barturen, I.; Jiménez-Díaz, M. B.; Mulet, T.; Rullas, J.; Herreros, E.; Ferrer, S.; Jiménez, E.; Mendoza, A.; Regadera, J.; Rosenthal, P. J.; Bathurst, I.; Pompliano, D. L.; Gómez de las Heras, F.; Gargallo-Viola, D. A murine model of falciparum-malaria by in vivo selection of competent strains in non-myelodepleted mice engrafted with human erythrocytes. *PLoS One* **2008**, *3*, No. e2252.
(68) Jiménez-Díaz, M. B.; Mulet, T.; Gómez, V.; Viera, S.; Alvarez, A.; Garuti, H.; Vázquez, Y.; Fernández AIbáñez, J.; Ibáñez, J.; Jiménez, M.; Jiménez, M.; Gargallo-Viola, D.; Gargallo-Viola, D.; Angulo-

https://doi.org/10.1021/acs.jmedchem.2c01336
J. Med. Chem. 2022, 65, 14121−14143

Barturen, I. Quantitative measurement of Plasmodium-infected erythrocytes in murine models of malaria by flow cytometry using bidimensional assessment of SYTO-16 fluorescence. *Cytometry, Part A* **2009**, *75A*, 225−235.
(69) Prado, M.; Eickel, N.; De Niz, M.; Heitmann, A.; Agop-Nersesian, C.; Wacker, R.; Schmuckli-Maurer, J.; Caldelari, R.; Janse, C. J.; Khan, S. M.; May, J.; Meyer, C. G.; Heussler, V. T. Long-term live imaging reveals cytosolic immune responses of host hepatocytes against Plasmodium infection and parasite escape mechanisms. *Autophagy* **2015**, *11*, 1561−1579.

https://doi.org/10.1021/acs.jmedchem.2c01336
J. Med. Chem. 2022, 65, 14121−14143